HHS Public Access

Author manuscript

Immunity. Author manuscript; available in PMC 2020 May 21.

Published in final edited form as:

Immunity. 2019 May 21; 50(5): 1218–1231.e5. doi:10.1016/j.immuni.2019.03.005.

Loss of Neurological Disease HSAN-I-Associated Gene *SPTLC2* Impairs CD8+ T Cell Responses to Infection by Inhibiting T Cell Metabolic Fitness

Jingxia Wu[1,18], **Sicong Ma**[1,16,18], **Roger Sandhoff**[2,18], **Yanan Ming**[3], **Agnes Hotz-Wagenblatt**[4], **Vincent Timmerman**[5], **Nathalie Bonello-Palot**[6], **Beate Schlotter-Weigel**[7], **Michaela Auer-Grumbach**[8], **Pavel Seeman**[9], **Wolfgang N. Löscher**[10], **Markus Reindl**[10], **Florian Weiss**[11], **Eric Mah**[12], **Nina Weisshaar**[1,17], **Alaa Madi**[1,17], **Kerstin Mohr**[1], **Tilo Schlimbach**[1], **Rubí M.-H. Velasco Cárdenas**[1], **Jonas Koeppel**[1], **Florian Grünschläger**[1], **Lisann Müller**[1], **Maren Baumeister**[1], **Britta Brügger**[13], **Michael Schmitt**[14], **Guido Wabnitz**[15], **Yvonne Samstag**[15], and **Guoliang Cui**[1,17,19,*]

[1]T Cell Metabolism Group (D140), German Cancer Research Center (DKFZ), Im Neuenheimer Feld 280, 69120 Heidelberg, Germany.

[2]Lipid Pathobiochemistry Group (G131), German Cancer Research Center (DKFZ), Im Neuenheimer Feld 280, 69120 Heidelberg, Germany.

[3]Internal Medicine IV, University Heidelberg Hospital, Im Neuenheimer Feld 345, 69120 Heidelberg, Germany.

[4]Core Facility Omics IT and Data Management, German Cancer Research Center (DKFZ), Im Neuenheimer Feld 280, 69120 Heidelberg, Germany.

[5]Peripheral Neuropathy Research Group, Department of Biomedical Sciences, Institute Born Bunge, B-2610, University of Antwerp, Antwerpen, Belgium

[6]Department of medical genetics, Children Timone hospital, 264 Rue Saint Pierre & Aix Marseille Univ, INSERM, MMG, U1251, 13385 Marseille, France.

[7]Friedrich-Baur-Institut, Neurologische Klinik and Poliklinik Ludwig-Maximilians-Universität, 80336, München

[8]Department of Orthopaedics and Trauma Surgery, Medical University of Vienna, Vienna, Austria

[*]Corresponding author: Guoliang Cui Ph.D. D140, German Cancer Research Center (DKFZ), Im Neuenheimer Feld 280, Heidelberg, Germany. Phone: +49 06221 42-1370. Fax: +49 06221 41 1715. g.cui@dkfz.de.

AUTHOR CONTRIBUTIONS

J.W., S.M., R.S., Y.M., V.T., N.B., B.S., M.A., P.S., W.L., M.R., F.W., E.M., B.B., M.S., G.W., Y.S. and G.C. designed the experiments. J.W. and S.M. did the majority of the biological experiments. R.S. performed the mass spectrometry analysis. N.W., A.M., K.M., T.S., Velasco Cárdenas RM, J.K., F.J., L.M., and M.B. assisted the three co-first authors in doing the experiments A.H. performed the bioinformatic analysis. G.C. wrote the manuscript.

DECLARATION OF INTERESTS

The authors declare no competing interests.

[9]DNA Laboratory, Department of Child Neurology, 2nd Medical School, Charles University and University Hospital Motol, Prague, Czech Republic

[10]Clinical Department of Neurology, Medical University Innsbruck, Anichstr. 35, 6020 Innsbruck, Austria

[11]Department of Psychiatry and Psychotherapy, University Hospital of Psychiatry, Bolligenstrasse 111, 3000 Bern, Germany

[12]School of Medicine, UC San Diego, 9500 Gilman Drive, La Jolla, CA 92093

[13]Heidelberg University Biochemistry Center (BZH), Im Neuenheimer Feld 328, Heidelberg, Germany.

[14]Internal Medicine V, University Heidelberg Hospital, Im Neuenheimer Feld 410, 69120, Heidelberg, Germany.

[15]Section Molecular Immunology, Institute of Immunology, Heidelberg University, Im Neuenheimer Feld 305, 69120 Heidelberg, Germany

[16]Medical Faculty Heidelberg, Heidelberg University, 69120 Heidelberg, Germany.

[17]Faculty of Biosciences, Heidelberg University, 69120 Heidelberg, Germany.

[18]Equal contribution

[19]Lead Contact

SUMMARY

Patients with the neurological disorder HSAN-I suffer frequent infections, attributed to a lack of pain sensation and failure to seek care for minor injuries. Whether protective $CD8^+$ T cells are affected in HSAN-I patients remains unknown. Here, we report that HSAN-I-associated mutations in serine palmitoyltransferase subunit *SPTLC2* dampened human T cell responses. Antigen stimulation and inflammation induced SPTLC2 expression, and murine T cell-specific ablation of *Sptlc2* impaired antiviral T cell expansion and effector function. *Sptlc2*-deficiency reduced sphingolipid biosynthetic flux and led to prolonged activation of the mechanistic target of rapamycin complex 1 (mTORC1), endoplasmic reticulum (ER) stress, and $CD8^+$ T cell death. Protective $CD8^+$ T cell responses in HSAN-I patient PBMCs and *Sptlc2*-deficient mice were restored by supplementing with sphingolipids and pharmacologically inhibiting ER stress-induced cell death. Therefore, SPTLC2 underpins protective immunity by translating extracellular stimuli into intracellular anabolic signals and antagonizes ER stress to promote T cell metabolic fitness.

In Brief

SPTLC2 mutations are associated with the neurological disorder HSAN-I, in which patients get frequent infections, attributed to loss of pain sensation and failure to seek treatment for minor injuries. Wu et al. show that protective $CD8^+$ T cell responses are defective in HSAN-I patients and that $CD8^+$ T cells require SPTLC2-mediated sphingolipid synthesis to promote T cell metabolic fitness.

Graphical Abstract

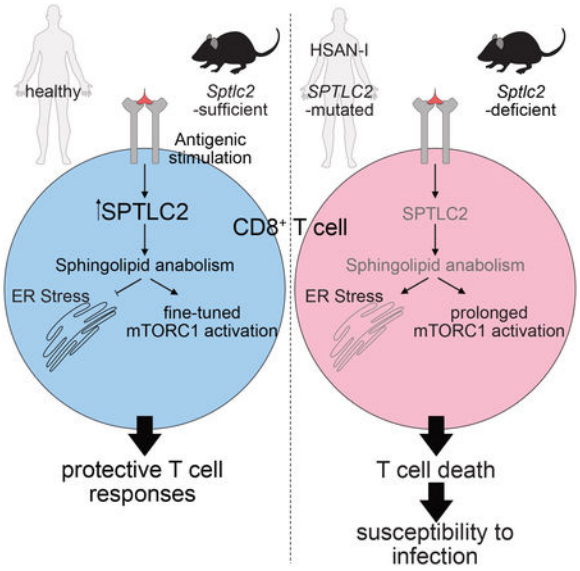

INTRODUCTION

Hereditary sensory neuropathy type 1 (HSAN-I) is a severe neurological disease that is characterized by neuron dysfunction and severe distal sensory loss. HSAN-I patients lose their sense of pain, and as a result, they often do not seek immediate medical treatment of minor injuries, which eventually develop into severe infections and ulcerations that may even necessitate amputations. HSAN-I has been shown to be associated with missense mutations in genes encoding the two subunits of serine palmitoyltransferase (SPT), SPT long chain base subunit 1 (*SPTLC1)* and *SPTLC2* (Bejaoui et al., 2001; Dawkins et al., 2001; Rotthier et al., 2010). SPT catalyzes the first step of the *de novo* synthesis of sphingolipids by condensing L-serine and palmitoyl-coenzyme A into 3-keto-sphinganine (3-KDS). 3-KDS can be further converted to the simple sphingoid bases, ceramides and complex sphingolipids. Missense mutations of SPT reduce its enzymatic activity, shift SPT substrate specificity and generate neurotoxic products (Alecu et al., 2017; Penno et al., 2010; Rotthier et al., 2010). Although SPT mutations are accompanied by severe infections in HSAN-I patients, it remains largely unknown if SPT directly regulates anti-infection $CD8^+$ T cell responses.

T cell responses to antigenic stimulation are accompanied by a metabolic reprogramming (Wang et al., 2011). Glucose and amino acids are metabolized to fuel bioenergetics and biosynthesis of macromolecules, such as lipids. Sphingolipids are an important group of structural lipids found in the plasma membrane with bioactive properties (Hannun and Obeid, 2008; Sandhoff, 1993). Accumulating evidence suggests that in addition to acting as building blocks for membrane biosynthesis, sphingolipids also regulate cellular signaling in immune cells. For example, sphingosine 1-phosphate (S1P) regulates T cell trafficking and modulates differentiation of regulatory T (Treg) cells and T helper 1 (Th1) cells (Kappos et al., 2010; Liu et al., 2009; Liu et al., 2010; Matloubian et al., 2004; Rivera et al., 2008). The ceramide synthase-6 deficiency protects mice from colitis development and T cell-induced graft-versus-host disease (Scheffel et al., 2017; Sofi et al., 2017). In addition, ceramides

decrease mitochondrial membrane potential and induce apoptosis (Arora et al., 1997; Di Paola et al., 2000; Ghafourifar et al., 1999; Siskind et al., 2002; Zamzami et al., 1995). Ceramides also suppress dendritic cell antigen uptake and presentation (Sallusto et al., 1996). On the other hand, ceramides enhance Treg cell suppressive function by activating protein phosphatase 2A (PP2A) and protein phosphatase 1 (PP1) and dephosphorylating mTOR (Apostolidis et al., 2016). Moreover, acid sphingomyelinase has been shown to promote the cytotoxic cytokine secretion from $CD8^+$ T cells (Herz et al., 2009). It remains incompletely understood how the simple sphingoid bases, such as sphinganine, regulate T cell responses to infectious diseases.

Here we analyzed *SPTLC2*-mutant T cells from HSAN-I patients and mouse models with T cell-specific deficiency of *Sptlc2*. *Sptlc2*-deficiency not only affected T cell sphingolipid anabolism but also led to a prolonged activation of the mechanistic target of rapamycin complex 1 (mTORC1), which caused endoplasmic reticulum (ER) stress and $CD8^+$ T cell death. Antiviral $CD8^+$ T cell survival and proliferation were restored in HSAN-I peripheral blood mononuclear cells (PBMCs) by supplementing sphingolipids and pharmacologically inhibiting ER stress-induced apoptosis. This study has provided an alternative explanation of the frequent infections observed in the HSAN-I patients, in which *SPTLC2* mutations directly affect T cell responses and anti-viral immunity. Our study has also revealed that SPTLC2 mediates antigenic stimulatory and inflammatory signals to instruct T cell sphingolipid anabolism, tailors mTORC1 activation to antagonize ER stress, maintains $CD8^+$ T cell metabolic fitness, and underpins protective immunity.

RESULTS

The SPTLC2 mutation affects HSAN-I patient $CD8^+$ T cell effector cytokine production, proliferation, and survival

To determine if HSAN-I-causing mutations in *SPTLC2* affected $CD8^+$ T cell responses, we analyzed the PBMCs from HSAN-I patients bearing point mutations (G435V or G382V) in *SPTLC2* and from age and gender-matched healthy subjects. The $CD4^+$ and $CD8^+$ T cell percentages of PBMCs were comparable between HSAN-I patients and healthy donors (Figure 1A). Using two surface markers CCR7 and CD45RA as previously reported (Romero et al., 2007), we found the percentages of naïve, effector and central memory T cell subsets were also similar between the two groups (Figure S1A–B). In addition, we detected no difference of the transcription factor Foxp3 protein expression or resting $CD8^+$ T cell survival between the two groups (Figure S1C–D). Effector cytokine production by HSAN-I $CD8^+$ T cells was significantly reduced (Figure 1B). Furthermore, HSAN-I $CD8^+$ T cells proliferated more slowly than healthy subject $CD8^+$ T cells upon T cell receptor (TCR) stimulation (Figure 1C). The reduction of T cell proliferation was associated with a significant increase of apoptosis (Figure 1D). Collectively, these results show that HSAN-I-causing *SPTLC2* mutations dampen human T cell effector cytokine production, proliferation, and survival.

Antigenic stimulation and inflammation induce SPTLC2 protein expression in CD8$^+$ T cells

To study the potential role of SPTLC2 in anti-infection T cell responses, we used a mouse model infected with lymphocytic choriomeningitis virus (LCMV)-Armstrong and monitored SPTLC2 expression in the LCMV-specific CD8$^+$ T cells. Briefly, TCR transgenic P14 CD8$^+$ T cells (P14 T cells recognize the LCMV $GP_{33–41}$ epitope) were adoptively transferred into congenically mismatched C57BL/6 mice, which were subsequently infected with LCMV. Six days after infection, we detected significantly higher protein levels of SPTLC2 in donor P14 CD8$^+$ T cells compared with those of naive P14 CD8$^+$ T cells (Figure 2A). $GP_{33–41}$ peptide, and to a lesser extent, inflammatory cytokines, induced the SPTLC2 expression of *in vitro* cultured P14 CD8$^+$ T cells (Figure 2B). These results suggest that both antigen exposure and inflammation promote SPTLC2 expression.

Sptlc2-deficiency impairs antiviral effector CD8$^+$ T cell formation

Inspired by the observation that SPTLC2 protein was upregulated in effector CD8$^+$ T cells, we went to explore if SPTLC2 was required for antiviral effector CD8$^+$ T cell differentiation. We created mice with T cell-specific deficiency of *Sptlc2* by breeding the *Cd4*-cre strain with the *Sptlc2*$^{Flox/Flox}$ strain (Li et al., 2009). *Sptlc2*$^{Flox/Flox}$*Cd4*-cre mice had similar numbers of total thymocytes and similar percentages of CD4 single positive (SP) cells, CD8$^+$ SP cells, and CD4$^+$CD8$^+$ cells compared with wildtype littermates (Figure S2A–B). CD4$^+$ and CD8$^+$ T cell numbers in the inguinal lymph nodes were comparable between wildtype and *Sptlc2*-deficient mice. Splenic CD4$^+$ T cell numbers were slightly reduced in *Sptlc2*-deficient mice but not statistically significant. Splenic CD8$^+$ T cell numbers of *Sptlc2*$^{Flox/Flox}$*Cd4*-cre mice were reduced compared with those of wildtype littermates (Figure S2A). The expression of CD69 and IL-7Rα was similar between *Sptlc2*-deficient and -sufficient CD8$^+$ T cells, whereas CD62L was modestly reduced (Figure S2C). These results reveal that *Sptlc2*-deficiency does not affect T cell thymic development and moderately reduces CD8$^+$ T cell numbers in the spleen but not lymph nodes under steady status.

To investigate if SPTLC2 protein regulated antiviral CD8$^+$ T cell responses, we infected *Sptlc2*$^{Flox/Flox}$*Cd4*-cre mice and wildtype littermates with LCMV. Eight days later, wildtype mice mounted a robust antiviral CD8$^+$ T cell response, characterized by the differentiation of tetramer-positive CD8$^+$ T cells (Figure 2C). *Sptlc2*-deficiency impaired the generation of LCMV-specific effector T cells, as manifested by the significant decrease of tetramer-positive CD8$^+$ T cell numbers and effector cytokine production (Figure 2C–D). Moreover, in line with the impaired antiviral CD8$^+$ T cell differentiation, the viral titers in serum and spleens were much higher in *Sptlc2*$^{Flox/Flox}$*Cd4*-cre mice compared with those in the wildtype littermates (Figure 2E–F). Taken together, these results demonstrate that SPTLC2 is essentially required for the formation of robust antiviral effector CD8$^+$ T cell responses.

SPTLC2 plays a CD8$^+$ T cell-intrinsic role in effector T cell formation

Because the expression of Cre under the control of *Cd4* deletes loxp-flanked genes in both CD4$^+$ and CD8$^+$ T cells (Lee et al., 2001; Sawada et al., 1994), we next addressed if SPTLC2 protein regulated antiviral T cell differentiation in a CD8$^+$ T cell-intrinsic manner. We crossed *Sptlc2*$^{Flox/Flox}$*Cd4*-cre mice to the TCR transgenic P14 mice. Then, we mixed

the *Sptlc2*$^{Flox/Flox}$*Cd4*-cre P14 CD8$^+$ T cells with P14 CD8$^+$ T cells from wildtype littermates before we adoptively transferred them into wildtype recipient mice (Figure 3A). We were able to distinguish between the congenically mismatched *Sptlc2*$^{+/+}$ and *Sptlc2*$^{Flox/Flox}$ donor CD8$^+$ T cells in the subsequent FACS analysis. Following LCMV infection, these P14 peripheral chimeric mice were sacrificed at different time points as indicated (Figure 3B). The *Sptlc2*-deficient and -sufficient P14 CD8$^+$ T cell numbers were comparable in the first 4 days after infection, suggesting that the initial T cell activation was similar between the two groups. However, the *Sptlc2*-deficient CD8$^+$ T cells were out-competed by their wildtype counterparts at day 6~8 (Figure 3C–D), accompanied by a significant increase of apoptosis (Figure 3E, F). In addition, SPTLC2 was required for the formation of the KLRG1^{hi}IL-7Rα^{lo} short-lived effector cells (SLECs) but not KLRG1^{lo}IL-7Rα^{hi} memory precursor effector cells (MPECs) (Joshi et al., 2007) (Figure 3E, G). Furthermore, effector cytokine production was also affected by *Sptlc2* deficiency (Figure 3E, H). Taken together, these data reveal that antiviral effector CD8$^+$ T cell responses require SPTLC2 in a cell-intrinsic manner.

Sptlc2-deficiency causes aberrant mTORC1 activation and ER stress in antiviral CD8$^+$ T cells

To study how *Sptlc2*-deficiency affected effector CD8$^+$ T cell formation, we went to analyze the global gene expression profiles of *Sptlc2*-deficient and -sufficient CD8$^+$ T cells. Briefly, we performed RNA sequencing (RNA-Seq) analysis of the CD8$^+$ T cells isolated from *Sptlc2*$^{Flox/Flox}$*Cd4*-cre or wildtype littermates before and 8 days after LCMV infection. There were only modest differences between *Sptlc2*-deficient and -sufficient CD8$^+$ T cell gene expression profiles before infection. Intriguingly, the transcriptional differences were remarkably increased at day 8 after LCMV infection, as manifested by the increased numbers of genes distributed outside of the dash lines (Figure 4A). Effector CD8$^+$ T cell hallmark genes, such as *Klrg1*, *Prdm1*, *Id2*, *Tbx21*, and *Ifng* were reduced in *Sptlc2*-deficient CD8$^+$ T cells (Figure 4B), echoing the observations that *Sptlc2*-deficiency impaired effector CD8$^+$ T cell responses (Figure 2). In addition, genes encoding ceramidases (*Asah1*, *Asah2*, and *Acer3*) and sphingosine phosphate lyase 1 (*Sgpl1*) were increased in *Sptlc2*-deficient cells, implying that the sphingoid base salvage pathways were enhanced presumably to compensate for the deficiency of the SPTLC2 protein-mediated *de novo* synthetic pathway (Kitatani et al., 2008; Tettamanti et al., 2003).

In addition, a group of genes regulating ER stress, such as C/EBP homologous protein (*CHOP*, also known as *Ddit3*), X-box-binding protein (*XBP*)-1, and binding of immunoglobulin protein (*Bip*, also known as *Hspa5*) were significantly increased in *Sptlc2*-deficient CD8$^+$ T cells (Figure 4B). Because *Sptlc2*-deficiency affected CD8$^+$ T cell subset differentiation at day 8, we monitored the mRNA levels of these genes by qPCR at an earlier time point and got similar results (Figure S3A–E). The subsequent Ingenuity Pathway Analysis (IPA) revealed that one top pathway upregulated in *Sptlc2*-deficient CD8$^+$ T cells was ER stress-induced apoptosis (Figure S3F). Western blot analysis confirmed that *Sptlc2*-deficient CD8$^+$ T cells expressed higher protein levels of ER stress markers, such as CHOP, XBP-1, Bip, phosphorylated eIF2α (peIF2α) and phosphorylated protein kinase RNA-like endoplasmic reticulum kinase (pPERK) (Figure 4D). Furthermore, *Sptlc2*-deficient CD8$^+$ T

cells displayed significantly dilated ER compared with the wildtype CD8$^+$ T cells (Figure S3G). Collectively, these data reveal that *Sptlc2*-deficiency causes ER stress in CD8$^+$ T cells.

We next explored the underlying mechanisms through which *Sptlc2*-deficiency caused ER stress. It has been reported that prolonged activation of mTORC1 and phosphorylation of S6 ribosomal protein (S6) causes ER stress (Di Nardo et al., 2009; Ozcan et al., 2008). Upon anti-CD3 and anti-CD28 stimulation, wildtype CD8$^+$ T cells rapidly increased S6 and 4E-BP1 phosphorylation (surrogate markers of mTORC1 activity), which dropped at a later time point (Figure 4C, S4A). In contrast to the short-term mTORC1 activation in wildtype CD8$^+$ T cells, *Sptlc2*-deficiency sustained S6 and 4E-BP1 phosphorylation for three days (Figure 4C, S4A). One might expect the enhancement of mTORC1 activity was dependent on Akt. However, we did not detect a change of Akt signaling. One explanation is that the mTORC1 activity is not dependent on PI3K/Akt activation in CD8$^+$ T cells (Finlay et al., 2012). Furthermore, *Sptlc2*-deficiency did not affect NFκB (p65), MAPK (p38, JNK, Erk) or NFAT1 signaling (Figure S2D–E). To dissect if the prolonged mTORC1 activation was required for ER stress in *Sptlc2*-deficient T cells, we treated the LCMV-infected *Sptlc2*$^{Flox/Flox}$*Cd4*-cre mice with mTORC1 inhibitor rapamycin. Remarkably, rapamycin reduced the expression of the ER stress markers (Figure 4D), indicating a causal relationship between the prolonged activation of mTORC1 and ER stress in *Sptlc2*-deficient CD8$^+$ T cells.

Sptlc2-deficiency reduces the sphingolipid biosynthetic flux and prolongs mTORC1 activation through protein phosphatases in CD8$^+$ T cells

Next, we examined how *Sptlc2*-deficiency prolonged mTORC1 activation in CD8$^+$ T cells. Sphingolipids have been shown to regulate mTORC1 activity (Apostolidis et al., 2016; Chung et al., 1997; Grey et al., 2002; Kluk and Hla, 2001). Thus, we hypothesize that the aberrant mTORC1 activation in *Sptlc2*-deficient T cells was due to dysregulated sphingolipid metabolism. To test this hypothesis, we analyzed the sphingolipid profiles of *Sptlc2*-sufficient and -deficient CD8$^+$ T cells. Sphinganine, dihydroceramide, ceramide, and sphingomyelin were all significantly reduced in *Sptlc2*-deficient T cells (Figure 5A and Table S1–2). On the other hand, 3-KDS was below the limit of detection. These data show that 3-KDS is probably a transient metabolic intermediate in mouse CD8$^+$ T cells. Sphingosine generation was unaffected in *Sptlc2*-deficient T cells (Figure 5A).

To examine how SPTLC2 protein regulated sphingolipid biosynthetic flux in *Sptlc2*-sufficient and -deficient CD8$^+$ T cells, we performed the isotope labeling experiment (Figure 5B–C and Table S1–2). Briefly, we pulsed the wildtype and *Sptlc2*-deficient CD8$^+$ T cells with $^{13}C_3$,^{15}N-labeled L-serine and then monitored the ^{13}C and ^{15} N-labeled metabolic intermediates over time. Similar to the quantification of the endogenous 3-KDS, ^{13}C and ^{15} N-labeled 3-KDS could not be detected, supporting that 3-KDS probably only existed transiently in T cells. The incorporation of isotope tracers into sphinganine and other sphingolipids became detectable as early as 30 minutes after $^{13}C_3$,^{15}N-labeled L-serine addition, and throughout the entire assay (Figure 5C). Furthermore, *Sptlc2*-deficiency reduced the biosynthesis of sphinganine, dihydroceramide, ceramide, and sphingomyelin.

Sptlc2-deficiency did not affect the incorporation of isotope tracers into sphingosine during the entire period of observation, which helped to explain the comparable levels of endogenous sphingosine between *Sptlc2*-sufficient and -deficient $CD8^+$ T cells (Figure 5A, C).

To test if HSAN-I-associated *SPTLC2* mutation influenced the canonical SPT activity in human $CD8^+$ T cells, we pulsed the resting and *in vitro* activated $CD8^+$ T cells of HSAN-I patients and healthy subjects with $^{13}C_3$,^{15}N-labeled L-serine for 60 minutes. Then we monitored the ^{13}C and ^{15}N incorporation into the downstream sphingolipids. Most of the sphingolipids examined in this assay, except ^{13}C,^{15}N-dihydroceramide and ^{13}C,^{15}N-ceramide, were only modestly affected by the *SPTLC2* mutation in resting $CD8^+$ T cells (Figure S1E). Compared with the resting healthy subject $CD8^+$ T cells, the activated healthy subject $CD8^+$ T cells incorporated much more ^{13}C and ^{15} N into sphingolipids, suggesting that T cell activation significantly enhanced the sphingolipid biosynthesis (Figure S1E). In contrast, HSAN-I patient T cells were resistant to the anti-CD2, anti-CD3 and anti-CD28-induced sphingolipid increase. As a result, the originally minimal difference of the SPT activity between the HSAN-I patient and healthy subject resting $CD8^+$ T cells was amplified by the T cell activation. Compared with the mouse $CD8^+$ T cell metabolic flux analysis, ^{13}C, ^{15}N-3KDS was detectable and ^{13}C,^{15}N-sphingosine was below the detection limit in the human $CD8^+$ T cells, suggesting a species-specific difference in the sphingolipid synthesis. Despite this minor difference, the data suggest that both *Sptlc2* genetic deficiency in mice and *SPTLC2* point mutation in human reduced the SPT activity in $CD8^+$ T cells.

To examine if the prolonged mTORC1 activation in *Sptlc2*-deficient T cells was due to the reduction of sphingolipid biosynthesis, we supplemented various sphingolipids into *Sptlc2*-deficient T cell culture. Supplementation of 3-KDS, sphinganine, dihydroceramide, ceramide, and sphingomyelin but not sphingosine reduced S6 phosphorylation and ER stress marker expression in *Sptlc2*-deficient $CD8^+$ T cells (Figure 5D, S4A and S5). Intriguingly, this pS6 suppression was blocked by microcystin-LR (an inhibitor of PP1 and PP2A) (Figure 5D), and the PP2A activity was significantly reduced in the *Sptlc2*-deficient cells (Figure S6A), suggesting that SPTLC2 prevented mTORC1 hyperactivation in $CD8^+$ T cells dependent on PP1 and PP2A. Ceramides have been shown to increase the PP2A activity through inhibiting the "Su(var)3–9, Enhancer-of-zeste and Trithorax" (SET)-domain containing protein inhibitor 2 of PP2A (I2PP2A, encoded by *Set*) (Dobrowsky et al., 1993; Li et al., 1996; Mukhopadhyay et al., 2009). To determine if *Sptlc2*-deficiency suppressed PP2A activity dependent on I2PP2A in $CD8^+$ T cells, we generated *Set*-deficient $CD8^+$ T cells through the electroporation-mediated delivery of CRISPR gRNA/Cas9 complex following a recently reported protocol (Seki and Rutz, 2018). The *Set*/*Sptlc2* dual deficient $CD8^+$ T cells had higher PP2A activity, reduced S6 phosphorylation and enhanced cell survival compared with the *Sptlc2*-deficient $CD8^+$ T cells (Figure S6B–E). Collectively, these results support the hypothesis that SPTLC2-mediated sphingolipid synthesis is required to maintain appropriate PP2A and mTORC1 activity through inhibiting I2PP2A (Figure S6F).

Sphingolipid supplementation and inhibition of ER stress-induced cell death partially restore Sptlc2-deficient antiviral T cell survival and expansion

Next, we tested if supplementation of sphingolipids and pharmacological inhibition of ER stress-induced cell death rescued the *Sptlc2*-deficient T cell survival and proliferation. We established an *in vitro* assay in which *Sptlc2*-deficient $CD8^+$ T cells underwent apoptosis and proliferated more slowly than wildtype control $CD8^+$ T cells upon stimulation with anti-CD3 and anti-CD28 (Figure 6A–B). These results also echoed the observation that *Sptlc2*-deficiency impaired $CD8^+$ T cell responses in the LCMV infection model (Figure 2C–F). Exogenous sphinganine restored cell survival and proliferation (Figure 6A–B). In addition, 3-KDS, sphingomyelin but not sphingosine partially rescued *Sptlc2*-deficient $CD8^+$ T cell survival and proliferation (Figure 6A–B and data not shown). This result correlated with the observation that sphingosine was not reduced in *Sptlc2*-deficient $CD8^+$ T cells (Figure 5A and 5C). In addition, salubrinal (an inhibitor of ER stress-induced cell death) (Boyce et al., 2005) fundamentally restored *Sptlc2*-deficient $CD8^+$ T cell survival and proliferation, suggesting that ER stress caused *Sptlc2*-deficient $CD8^+$ T cell death and proliferation defect. Furthermore, the pS6 protein level was still very high compared with that in the wildtype T cells (Figure S4B). These results suggest that the increased pS6 can be uncoupled from cell death in salubrinal-treated *Sptlc2*-deficient $CD8^+$ T cells. In addition, rapamycin enhanced *Sptlc2*-deficient $CD8^+$ T cell survival and but only moderately increased cell proliferation (Figure 6A–B), suggesting that although mTORC1 hyperactivation causes cell death, mTORC1 activity is still required for the optimal proliferation of *Sptlc2*-deficient $CD8^+$ T cells.

To test if sphingolipid administration and ER stress-induced cell death inhibition rescued *Sptlc2*-deficient antiviral $CD8^+$ T cell responses *in vivo*, we adoptively transferred *Sptlc2*$^{Flox/Flox}$*Cd4*-cre and wildtype P14 $CD8^+$ T cells into wildtype recipient mice. These "P14 peripheral chimeras" were infected with LCMV-Armstrong and treated with sphinganine, rapamycin, salubrinal, or vehicle control. Intriguingly, sphinganine, and to a lesser extent, rapamycin and salubrinal treatment increased the numbers of *Sptlc2*-deficient $CD8^+$ T cell donors (Figure 6C–E). The administration of the three compounds also partially restored *Sptlc2*-deficient $CD8^+$ T cell survival, SLEC differentiation and effector cytokine production (Figure 6F). Collectively, these results indicate that *Sptlc2*-deficient effector $CD8^+$ T cell formation can be at least partially rescued by supplementing exogenous sphingolipids and inhibiting ER stress-induced cell death.

Sphingolipid supplementation and inhibition of ER stress-induced cell death enhances the SPTLC2-mutated HSAN-I patient $CD8^+$ T cell cytokine production, proliferation, and survival

To study if the findings made using the mouse models were relevant to the immunodeficiency observed in the HSAN-I patients, we supplemented sphinganine, rapamycin and salubrinal to $CD8^+$ T cells of the HSAN-I patients or healthy subjects. Sphinganine and salubrinal restored HSAN-I $CD8^+$ T cell effector cytokine production, cell proliferation, and survival (Figure 7). Rapamycin also increased HSAN-I $CD8^+$ T cell effector cytokine percentages and promoted cell survival. Compared with sphinganine and salubrinal, rapamycin only modestly but still significantly enhanced HSAN-I $CD8^+$ T cell

proliferation (Figure 7). Taken together, these results suggest that sphingolipid supplementation and ER stress inhibition at least partially correct the HSAN-I-associated immunodeficiency.

Deoxysphingolipids suppress CD8$^+$ T cell proliferation and cytokine production at high concentrations

In addition to reducing the SPT enzymatic activity, the HSAN-I-associated *SPTLC2* mutations also shift the substrate preference from L-serine to L-alanine and L-glycine, resulting in the production of neurotoxic 1-deoxysphinganine (m18:0), 1-deoxymethylsphinganine (m17:0) and downstream deoxysphingolipids (Alecu et al., 2017; Penno et al., 2010; Rotthier et al., 2010). To address if the neurotoxic deoxysphingolipids suppressed human CD8$^+$ T cell proliferation and cytokine production, we cultured healthy human CD8$^+$ T cells with two neurotoxic deoxysphingolipids, 1-deoxysphinganine (m18:0) and 1-deoxymethylsphinganine (m17:0) (Penno et al., 2010). We observed that the neurotoxic deoxysphingolipids suppressed human CD8$^+$ T cell proliferation and effector cytokine production when added at high concentrations (>2.4 μM) (Figure S7A–D). The previous studies suggest that the concentrations of 1-deoxysphinganine (m18:0) and 1-deoxymethylsphinganine (m17:0) in the plasma of HSAN-I patients are lower than 0.8 μM (Murphy et al., 2013; Penno et al., 2010). Thus, these data suggest that the deoxysphingolipids, at the concentrations observed in the HSAN-I patient plasma, do not exert cytotoxicity on CD8$^+$ T cells.

DISCUSSION

Investigations of rare human diseases, such as severe combined immunodeficiency (SCID), have revealed the importance of several key immunological pathways (Kovanen and Leonard, 2004; Leonard, 1996). Similarly, our finding of SPTLC2 as an immunometabolic checkpoint is a lesson learned from the rare neurological disorder HSAN-I. The current explanation for the frequent infections associated with HSAN-I is that the patients have a complete or partial loss of pain, and therefore do not seek immediate medical treatment of originally minor injuries. Our study has proposed a different mechanism that HSANI-associated genetic mutations in *SPTLC2* directly affect T cell responses. Besides *SPTLC2*, HSAN-I neuropathy has been revealed to be genetically linked to mutations other genes, such as *SPTLC1* (Bejaoui et al., 2001; Dawkins et al., 2001). Our unpublished data suggested that SPTLC1, similar to SPTLC2, was upregulated in CD8$^+$ T cells upon LCMV infection, implying that SPTLC1 might also regulate antiviral T cell responses in the form of a heterodimeric complex with SPTLC2. Thus, our study has provided a molecular mechanism linking HSAN-I neuropathy to the impaired T cell metabolism, survival, and function. This link will help us to better understand the causes of the HSAN-I clinical symptoms, and provide a different view of HSAN-I and also other ulceromutilating neuropathies from an immunological perspective.

The HSAN-I-associated *SPTLC2* mutations not only reduce SPT enzymatic activity but also shift the substrate preference from L-serine to L-alanine and L-glycine, resulting in the production of neurotoxic deoxysphingolipids (Alecu et al., 2017; Penno et al., 2010;

Rotthier et al., 2010). It has been shown in a pilot study that L-serine ameliorates clinical symptoms in HSAN-I patients (Garofalo et al., 2011). A clinical trial has been carried out by the same group (NCT01733407). The rationale is to increase the availability of L-serine and also to reduce the relative abundance of alanine and glycine for the synthesis of the neurotoxic products. Our study suggests sphinganine supplementation as another potential option to rescue the anti-infection T cell-intrinsic defects associated with HSAN-I. One future direction is to explore if sphinganine alone, or in combination with L-serine, ameliorates the HSAN-I clinical symptoms.

Sphingolipid metabolism has been implicated in the regulation of cell death and survival. For example, ceramides can induce cell cycle arrest and apoptosis by promoting the formation of large lipid raft signaling platforms, CD95 clustering, phosphatase activation and increasing the mitochondrial membrane permeability (Cremesti et al., 2001; Grassmé et al., 2001; Nickels and Broach, 1996; Siskind et al., 2002, 2006). On the other hand, sphingosine-1-phosphate induces Erk activation and antagonizes ceramides-induced SAPK/JNK pathway to promote cell survival (Cuvillier et al., 1996). Our current study has revealed another layer of complexity that sphinganine and other sphingolipids promoted effector $CD8^+$ T cell proliferation not only by fueling lipid anabolism but also through moderating mTORC1 activity and suppressing ER stress-induced cell death. mTORC1 activation plays an essential role in regulating cell growth and T cell metabolic reprogramming (Albert and Hall, 2015; Laplante and Sabatini, 2012; Wang et al., 2011; Zeng et al., 2013). Our study suggests that in spite of its importance in underpinning cell survival and growth, mTORC1 is tightly regulated to reduce ER stress and effector $CD8^+$ T cell death. Induced by TCR stimulation and inflammation, SPTLC2 instructs sphingolipid biosynthetic flux, fine-tunes infection-induced mTORC1 activity, and antagonizes ER stress-induced antiviral $CD8^+$ T cell death. Thus, SPTLC2 promotes T cell metabolic fitness and helps to maintain the sustainability of mTORC1-dependent metabolic reprogramming of antiviral effector $CD8^+$ T cells.

We found that *Sptlc2*-deficiency reduces the biosynthesis of sphinganine, dihydroceramide, ceramide, and sphingomyelin, but does not completely inhibit sphingolipid synthesis and barely affects sphingosine synthesis. This is in accordance with previous findings of residual sphingolipids in targeted cells and organs of other cell-specific *Sptlc2*-deficient mice (Chakraborty et al., 2013; Lee et al., 2012; Lee et al., 2017; Li et al., 2018; Li et al., 2009). One possibility is that the residual SPT activity of SPTLC1 suffices for low levels of sphingolipid synthesis. Another possibility is that sphingolipid metabolism is highly plastic. The influence of a single enzymatic defect in sphingolipid biosynthesis could be compensated by the changes of other metabolic steps; especially, if cells could take up sphingolipids from their environment, e.g. from exosomes. In addition, sphingolipid salvage pathways can also compensate for the deficiency of the *de novo* synthetic pathway. For example, sphingoid bases can be generated through degradation of the phosphorylated sphingoid bases by sphingosine phosphate lyase 1, which is encoded by *Sgpl1*. Remarkably, *Sptlc2*-deficient $CD8^+$ T cells expressed higher levels of *Sgpl1* mRNA. On the other hand, sphingosine can be generated through ceramide deacylation by ceramidases. Ceramidase-encoding genes such as *Asah1*, *Asah2*, and *Acer3* were increased in *Sptlc2*-deficient T cells. This altered gene expression pattern is expected to desensitize sphingosine biosynthesis

from the shrinking of ceramide intracellular pool in *Sptlc2*-deficient T cells. This metabolic plasticity is particularly important for T cells, because the sphingosine-derived metabolite sphingosine-1-phosphate plays an important role in T cell migration, differentiation, and proliferation (Cyster and Schwab, 2012; Jin et al., 2003; Liu et al., 2009; Liu et al., 2010; Mendoza et al., 2017).

Sptlc2-deficiency reduced antiviral $CD8^+$ T cell numbers more potently in the $Sptlc2^{Flox/Flox}Cd4$-cre mice than in the "P14 peripheral chimeras". One explanation is that both $CD4^+$ and $CD8^+$ T cells lack functional SPTLC2 in $Sptlc2^{Flox/Flox}Cd4$-cre mice, whereas in the "P14 peripheral chimeras", SPTLC2 remains intact in the host $CD4^+$ T cells. Our unpublished data suggest that SPTLC2 also regulates $CD4^+$ T cell subset differentiation. Because $CD4^+$ T cell help plays an important role in $CD8^+$ T cell primary response (Bennett et al., 1998; Bennett et al., 1997; Oh et al., 2008; Ridge et al., 1998; Schoenberger et al., 1998; Sokke Umeshappa et al., 2012; Wilson and Livingstone, 2008), the dual deficiency of *Sptlc2* in both $CD4^+$ and $CD8^+$ T cells is expected to influence antiviral $CD8^+$ T cells through both $CD8^+$ T cell-intrinsic and -extrinsic mechanisms in $Sptlc2^{Flox/Flox}Cd4$-cre mice. To study the $CD8^+$ T cell-extrinsic mechanisms, one future direction is to address the potential role of SPTLC2 in $CD4^+$ T cell subset differentiation and function.

Overall, our study has revealed that antiviral $CD8^+$ T cell responses required SPTLC2-mediated sphingolipid biosynthesis to support T cell anabolism and to reduce ER stress. These findings have also provided an immunological perspective to revisit the causes of human ulceromutilating neuropathies.

STAR ★ METHODS

CONTACT FOR REAGENTS AND RESOURCE SHARING

Further information and requests for resources and reagents should be directed to and will be fulfilled by the Lead Contact, Guoliang Cui (g.cui@dkfz.de).

EXPERIMENTAL MODEL AND SUBJECT DETAILS

Mice—$Sptlc2^{Flox/Flox}$ mice were kindly provided by Professor Xian-cheng Jiang (SUNY Downstate Medical Center, New York) via Professor Vishwa Dixit and Professor Susan Kaech (Yale University, New Haven) (Li et al., 2009). Mice were maintained in the German cancer research center (DKFZ) specific pathogen-free facility. We used sex-matched 6~10-week-old mice (both female and male) for the experiments and subsequent comparisons. All the studies were performed in accordance with DKFZ regulations after approval by the German regional council at the Regierungspräsidium Karlsruhe.

Human samples—The HSAN-I study was approved by the ethics committee of DKFZ and Heidelberg University. Informed consent from all patients was obtained before the analysis. HSAN-I human samples (4 female and 6 male at the age of 52.0±12.4) were collected by Drs. Nathalie Bonello-Palot, Beate Schlotter-Weigel, Michaela Auer-Grumbach, Pavel Seeman, Wolfgang Löscher, Markus Reindl, Eric Mah, David Boyle, Andre A Matti and Carla Grosmann. The patients did not have recent medical events related to their diagnosis.

METHOD DETAILS

LCMV infection—In infection-related experiments, mice were intraperitoneally infected with 2×10^5 pfu LCMV-Armstrong. Where indicated, we generated the "P14 chimeric mice" by adoptively transferring 10^4 LCMV-specific *Sptlc2*-sufficient and -deficient P14 TCR transgenic $CD8^+$ cells to C57BL/6 mice 1 day before LCMV-Armstrong infection. Mice were intraperitoneally treated with sphinganine (100 μg/kg body weight, every other day), rapamycin (100 μg/kg body weight, every other day), and salubrinal (1 mg/kg body weight, every other day).

Primary cell cultures—Primary T cells derived from gender-matched human subjects or mice (both male and female) were cultured in complete RPMI 1640 medium (plain RPMI 1640 medium with 10% fetal bovine serum, Penicillin and Streptomycin, 2-mercaptoethanol, L-Glutamine and non-essential amino acids). Antibodies, cytokines, peptides, and chemicals were supplemented as indicated. For the *in vitro* treatment with ceramides, C16 ceramide and C18 dihydroceramide were first dissolved in ethanol. Then 2% dodecane was added to increase the solubility as reported (Chalfant et al., 1999; Novgorodov et al., 2008). The final concentrations of dodecane and ethanol did not exceed 0.001% and 0.05% in the cell culture. 3-ketosphinganine (final concentration is 5 μM), sphinganine (5 μM), sphingosine (1 μM), and salubrinal (5 μM) were dissolved in DMSO. Sphingomyelin was dissolved in ethanol (10mg/ml) and the final working concentration was 4 μg/ml. Microcystin-LR dissolved in DMSO was added to cell culture medium at 25 nM. The stock solutions were warmed to 37°C prior to supplementation into the medium. Vehicle controls (DMSO or ethanol) were added with the final concentrations lower than 0.05%.

Lipid extraction from T cells—*Sptlc2*-sufficient and -deficient P14 $CD8^+$ T cells were activated with $GP_{33–41}$ peptide for three days and then stimulated with IL-2 for another two days. $CD8^+$ T cells were then pulsed with 500 μM $^{13}C_3$, ^{15}N-LSerine (Sigma) in HBSS plus 1% FBS at 37°C for 0–120 minutes. Then 2×10^7 cells were pelleted and used for lipid extraction. 100 μL of a methanolic solution containing a mix of internal lipid standards [C12–3-ketosphinganine, C20-sphinganine, C20-sphingosine, Cer(d18:1/14:0), Cer(d18:1/19:0), Cer(d18:1/25:0), Cer(d18:1/31:0), 1-desoxy-Cer(d18:0/12:0), GlcCer(d18:1/14:0), GlcCer(d18:1/19:0), GlcCer(d18:1/25:0), GalCer(d18:1/31:0), SM(d18:1/12:0), SM(d18:1/17:0), SM(d18:1/py), and SM(d18:1/31:0)] was added and further suspended in 400 μL chloroform:methanol (1:1). The suspension was incubated for 15 min at 37 °C in an ultrasound bath, which was turned on for 3 min in the beginning, after 5 and after 10 min. The suspension was centrifuged at room temperature at 13000g for 3 min and 450 μL of the clear supernatant was collected with a Hamilton syringe into a clean glass vial. The residual pellet was mixed with 450 μL of chloroform:methanol:water (10:10:1) treated like before and the second supernatant was added to the first. This extraction was repeated with the residual pellet and the third supernatant added to the other two. The pooled extract was dried with a gentle nitrogen gas stream at 37 °C and suspended in 2mL 100 mM aqueous potassium acetate using ultrasound for subsequent desalting via C18-reversed phase cartridges. The lipid eluate from the cartridges was dried and finally taken up in 200 μL 95% methanol and subjected to UPLC-ESI-MS^2 analysis. To detect sphingomyelins in the absence of phosphatidylserines an aliquot of the samples was dried and treated with 25%

aqueous ammonia:methanol (1:1) at 80 °C for 5 h. After drying samples with a gentle nitrogen stream at 40 °C, samples were taken up in 200 μl 95% methanol for LC-MS^2 analysis.

LC-MS^2 analysis of sphingolipids—Extracted lipids were separated on a Waters I class UPLC equipped with a Waters CSH C18 column (length 100 mm, diameter 2.1mm, particle size 1.7 μm) using a gradient starting with 57% solvent A (50% methanol, 50% water) and 43 % solvent B (99% 2-propanol, 1% methanol), both solvents containing 10 mM ammonium formiate, 0.1% formic acid and 5 μM sodium citrate. For details see Table S1. The UPLC was coupled to an ESI-(QqQ)-tandem mass spectrometer (Waters Xevo TQ-S) for compound detection in +ESI MRM mode. De novo synthesized SLs were discriminated from steady state SLs by incorporation of $^{13}C_3$,$^{15}N_1$-stable isotope labeled L-serine leading to an n+3 mass shift of the corresponding molecular ions and a corresponding n+2/n+3 mass shift of the product ions in MRM mode. For details see Table S2. Samples were injected and processed using MassLynx software, whereas mass spectrometric peaks were quantified according to their peak area ratio with respect to the internal standard using TargetLynx software (both v 4.1 SCN 843) both from Waters Corporation (Manchester, UK). Subsequently, quantification of ceramides, hexosylceramides, and sphingomyelins was adjusted to the length of the acyl-chain and dihydro(hexosyl)ceramide quantification was further adjusted by a factor calculated between the intensities external ceramides and dihydroceramidstandards of the same concentration.

Flow Cytometry—For Annexin V/propidium iodide (PI) staining, cells were washed with Annexin V buffer before staining with anti-Annexin V and PI. Cells were directly analyzed using LSR II without fixation. To stain surface antigens, cells were washed with FACS buffer before adding the fluorescently-conjugated antibodies. After incubating with antibodies for 20~30 minutes on ice, cells were washed with FACS buffer and fixed with 4% PFA. To stain cytokines, cells were permeabilized using the eBioscience permeabilization buffer. To stain phosphorylated antigens, cells were fixed with 4% PFA first. Then cells were treated with cold 70% methanol on ice for 30 minutes. After washing three times using FACS buffer, cells were incubated with staining antibodies on ice for 30 minutes before LSR II analysis. To do Celltrace Violet dilution assay, cells were labeled with Celltrace Violet in complete medium at 37°C for 20 minutes. Then cells were washed with RPMI 1640 medium with 1% FBS for 3 times. After 3 days, Celltracer Violet fluorescence was analyzed in the PacBlue channel using an LSR II.

Immunoblot—Cells were lysed using RIPA lysis buffer (150 mM NaCl, 1% NP-40, 0.5% sodium deoxycholate, 0.1% SDS and 50 mM Tris pH 8.0) and boiled in 5x SDS sample buffer (10% SDS, 10 mM DTT, 20% glycerol, 200 mM Tris-HCl, pH 6.8 and 0.05% bromophenol blue) for 5~10 minutes. Then cell lysates were loaded and resolved using 12% SDS-PAGE (120 V, until the blue indicator runs to the edge of the gel). Proteins were then transferred onto PVDF membranes (100 V, 1 hour, on ice). The membranes were then blocked with 5% milk in PBS supplemented with Tween-20 (PBST) for 1 hour at room temperature, followed by incubation overnight at 4°C with primary antibodies. The PVDF membrane was washed 3 times (5~10 minutes each time) with PBST and then incubated

with HRP-conjugated secondary antibodies at room temperature for 1 hour. After extensive washing with PBST, the membrane was developed using the ECL method. We quantified the band intensities using the NIH ImageJ program.

RNA sequencing—$CD8^+$ T cells were MACS-purified from naïve or LCMV-Armstrong-infected (2×10^5 pfu, day 8 after infection, i.p.) *Sptlc2*$^{Flox/Flox}$*Cd4*-cre mice and wildtype littermates. The purity of $CD8^+$ T cells was checked using FACS and it was higher than 96%. RNA was prepared using the QIAGEN RNeasy Mini Kit. DNA was removed using the QIAGEN RNase-Free DNase Set. Library was prepared by German cancer research center High Throughput Sequencing Unit. Then, libraries were pooled with six samples in each lane and sequenced (Illumina HiSeq 2000 v4 Single-Read 50 bp). For all samples, low quality bases were removed with Fastq_quality_filter from the FASTX Toolkit 0.0.13 (http://hannonlab.cshl.edu/fastx_toolkit/index.html) with 90% of the read needing a quality phred score > 20. Homertools 4.7 (Heinz et al., 2010) were used for PolyA-tail trimming, and reads with a length < 17 were removed. PicardTools 1.78 (https://broadinstitute.github.io/picard/) were used to compute the quality metrics with CollectRNASeqMetrics. With STAR 2.3 (Dobin et al., 2013), the filtered reads were mapped against mouse genome 38 (mm10) using default parameters. Count data were generated using featureCounts (Liao et al., 2014) (parameters --minReadOverlap 3 -T 3 -M -O) for the genes annotated in the gencode.vM16.gtf file. For the comparison with DESeq2 (Love et al., 2014), the input tables containing the replicates for groups to compare were created by a custom perl script. For DESeq2, DESeqDataSetFromMatrix was applied, followed by estimateSizeFactors, estimateDispersions, and nbinomWald testing. The result tables were annotated with gene information (gene symbol) derived from the gencode.vM8.gtf file. We then further analyze the RNA sequencing results using the Ingenuity Pathway Analysis (IPA, QIAGEN). The accession number of the RNA sequencing data is GSE112715 and available at Genome Expression Omnibus.

QUANTIFICATION AND DATA ANALYSIS

Statistical Analysis—All the data were presented as mean ± SD (error bar) unless otherwise specified. Where indicated, p values were determined by a two-tailed Student's t-test. We used GraphPad Prims (v 7.0.3) to do the statistical analysis. $p<0.05$ was considered statistically significant.

DATA AND SOFTWARE AVAILABILITY

The GEO accession number for the RNA sequencing is GSE112715.

Supplementary Material

Refer to Web version on PubMed Central for supplementary material.

ACKNOWLEDGMENTS

We thank the DKFZ core facilities (mouse work, flow cytometry, biosafety, monoclonal antibody and genomics) for the assistance. We thank Drs. Karsten Richter and Michelle Nessling for their help with the EM imaging. We thank Drs. Carla Grosmann, David Boyle and Andre A Matti for helping with the human sample collection. We thank Drs. Hermann-Josef Gröne, Walee Chamulitrat, and Hongying Gan-Schreier for discussions. We thank Dr. Xian-

cheng Jiang (SUNY Downstate Medical Center, New York) for providing the *Sptlc2*$^{Flox/Flox}$ mice. LCMV was provided by Dr. Susan Kaech (Yale University, New Haven, Connecticut). We also thank NIH core facility for kindly providing the LCMV tetramers. Guoliang Cui is supported by a Helmholtz Young Investigator Award (VH-NG-1113), German Research Foundation (DFG, CU375/5–1), German Cancer Aid Foundation (DKH, 70113343), Helmholtz AMPro, Rare Disease Foundation and BC Children's Hospital Foundation (#2286 and #2604). Sicong Ma is supported by a Chinese Scholar Council fellowship. Vincent Timmerman is supported by the Fund for Scientific Research (FWO-Flanders), Medical Foundation Queen Elisabeth (GSKE), Association Belge contre les Maladies Neuromusculaires (ABMM) and H2020 grant Solve-RD, 'Solving the unsolved rare diseases' under grant agreement 2017–779257. Pavel Seeman is supported by Ministry of Health of the Czech Republic AZV 16–30206A and DRO 00064203. This work was supported by the Austrian Science Fund (FWF, P27634FW, to M. A.-G.) and ÖNB (Nr.16880, to M. A.-G.). Eric Mah is supported by the US National Institutes of Health (NIH) grant UL1TR001442 awarded to UC San Diego Altman Clinical & Translational Research Institute (ACTRI). Britta Brügger is supported by the German Research Foundation (278001972 - TRR 186).

REFERENCE

Albert V, and Hall MN (2015). mTOR signaling in cellular and organismal energetics. Curr Opin Cell Biol 33, 55–66. [PubMed: 25554914]

Alecu I, Tedeschi A, Behler N, Wunderling K, Lamberz C, Lauterbach MAR, Gaebler A, Ernst D, Van Veldhoven PP, Al-Amoudi A, et al. (2017). Localization of 1-deoxysphingolipids to mitochondria induces mitochondrial dysfunction. Journal of lipid research 58, 42–59. [PubMed: 27881717]

Apostolidis SA, Rodriguez-Rodriguez N, Suarez-Fueyo A, Dioufa N, Ozcan E, Crispin JC, Tsokos MG, and Tsokos GC (2016). Phosphatase PP2A is requisite for the function of regulatory T cells. Nature immunology 17, 556–564. [PubMed: 26974206]

Arora AS, Jones BJ, Patel TC, Bronk SF, and Gores GJ (1997). Ceramide induces hepatocyte cell death through disruption of mitochondrial function in the rat. Hepatology 25, 958–963. [PubMed: 9096604]

Bejaoui K, Wu C, Scheffler MD, Haan G, Ashby P, Wu L, de Jong P, and Brown RH Jr. (2001). SPTLC1 is mutated in hereditary sensory neuropathy, type 1. Nature genetics 27, 261–262. [PubMed: 11242106]

Bennett SR, Carbone FR, Karamalis F, Flavell RA, Miller JF, and Heath WR (1998). Help for cytotoxic-T-cell responses is mediated by CD40 signalling. Nature 393, 478–480. [PubMed: 9624004]

Bennett SR, Carbone FR, Karamalis F, Miller JF, and Heath WR (1997). Induction of a CD8+ cytotoxic T lymphocyte response by cross-priming requires cognate CD4+ T cell help. The Journal of experimental medicine 186, 65–70. [PubMed: 9206998]

Boyce M, Bryant KF, Jousse C, Long K, Harding HP, Scheuner D, Kaufman RJ, Ma D, Coen DM, Ron D, and Yuan J (2005). A Selective Inhibitor of eIF2α Dephosphorylation Protects Cells from ER Stress. Science 307, 935–939. [PubMed: 15705855]

Chakraborty M, Lou C, Huan C, Kuo MS, Park TS, Cao G, and Jiang XC (2013). Myeloid cell-specific serine palmitoyltransferase subunit 2 haploinsufficiency reduces murine atherosclerosis. The Journal of clinical investigation 123, 1784–1797. [PubMed: 23549085]

Chalfant CE, Kishikawa K, Mumby MC, Kamibayashi C, Bielawska A, and Hannun YA (1999). Long Chain Ceramides Activate Protein Phosphatase-1 and Protein Phosphatase-2A: ACTIVATION IS STEREOSPECIFIC AND REGULATED BY PHOSPHATIDIC ACID. Journal of Biological Chemistry 274, 20313–20317. [PubMed: 10400653]

Chung T, Crilly KS, Anderson WH, Mukherjee JJ, and Kiss Z (1997). ATP-dependent Choline Phosphate-induced Mitogenesis in Fibroblasts Involves Activation of pp70 S6 Kinase and Phosphatidylinositol 3′-Kinase through an Extracellular Site: SYNERGISTIC MITOGENIC EFFECTS OF CHOLINE PHOSPHATE AND SPHINGOSINE 1-PHOSPHATE. Journal of Biological Chemistry 272, 3064–3072. [PubMed: 9006957]

Cremesti A, Paris F, Grassme H, Holler N, Tschopp J, Fuks Z, Gulbins E, and Kolesnick R (2001). Ceramide enables fas to cap and kill. The Journal of biological chemistry 276, 23954–23961. [PubMed: 11287428]

Cuvillier O, Pirianov G, Kleuser B, Vanek PG, Coso OA, Gutkind S, and Spiegel S (1996). Suppression of ceramide-mediated programmed cell death by sphingosine-1-phosphate. Nature 381, 800–803. [PubMed: 8657285]

Cyster JG, and Schwab SR (2012). Sphingosine-1-phosphate and lymphocyte egress from lymphoid organs. Annual review of immunology 30, 69–94.

Dawkins JL, Hulme DJ, Brahmbhatt SB, Auer-Grumbach M, and Nicholson GA (2001). Mutations in SPTLC1, encoding serine palmitoyltransferase, long chain base subunit-1, cause hereditary sensory neuropathy type I. Nature genetics 27, 309–312. [PubMed: 11242114]

Di Nardo A, Kramvis I, Cho N, Sadowski A, Meikle L, Kwiatkowski DJ, and Sahin M (2009). Tuberous sclerosis complex activity is required to control neuronal stress responses in an mTOR-dependent manner. The Journal of neuroscience: the official journal of the Society for Neuroscience 29, 5926–5937. [PubMed: 19420259]

Di Paola M, Cocco T, and Lorusso M (2000). Ceramide Interaction with the Respiratory Chain of Heart Mitochondria. Biochemistry 39, 6660–6668. [PubMed: 10828984]

Dobin A, Davis CA, Schlesinger F, Drenkow J, Zaleski C, Jha S, Batut P, Chaisson M, and Gingeras TR (2013). STAR: ultrafast universal RNA-seq aligner. Bioinformatics 29, 15–21. [PubMed: 23104886]

Dobrowsky RT, Kamibayashi C, Mumby MC, and Hannun YA (1993). Ceramide activates heterotrimeric protein phosphatase 2A. The Journal of biological chemistry 268, 15523–15530. [PubMed: 8393446]

Dutko FJ, and Oldstone MB (1983). Genomic and Biological Variation among Commonly Used Lymphocytic Choriomeningitis Virus Strains The Journal of general virology 64, 10.

Finlay DK, Rosenzweig E, Sinclair LV, Feijoo-Carnero C, Hukelmann JL, Rolf J, Panteleyev AA, Okkenhaug K, and Cantrell DA (2012). PDK1 regulation of mTOR and hypoxia-inducible factor 1 integrate metabolism and migration of CD8+ T cells. The Journal of experimental medicine 209, 2441–2453. [PubMed: 23183047]

Garofalo K, Penno A, Schmidt BP, Lee HJ, Frosch MP, von Eckardstein A, Brown RH, Hornemann T, and Eichler FS (2011). Oral L-serine supplementation reduces production of neurotoxic deoxysphingolipids in mice and humans with hereditary sensory autonomic neuropathy type 1. The Journal of clinical investigation 121, 4735–4745. [PubMed: 22045570]

Ghafourifar P, Klein SD, Schucht O, Schenk U, Pruschy M, Rocha S, and Richter C (1999). Ceramide Induces Cytochrome c Release from Isolated Mitochondria: IMPORTANCE OF MITOCHONDRIAL REDOX STATE. Journal of Biological Chemistry 274, 6080–6084. [PubMed: 10037689]

Grassmé H, Jekle A, Riehle A, Schwarz H, Berger J, Sandhoff K, Kolesnick R, and Gulbins E (2001). CD95 Signaling via Ceramide-rich Membrane Rafts. Journal of Biological Chemistry 276, 20589–20596. [PubMed: 11279185]

Grey A, Chen Q, Callon K, Xu X, Reid IR, and Cornish J (2002). The Phospholipids Sphingosine-1-Phosphate and Lysophosphatidic Acid Prevent Apoptosis in Osteoblastic Cells via a Signaling Pathway Involving Gi Proteins and Phosphatidylinositol-3 Kinase. Endocrinology 143, 4755–4763. [PubMed: 12446603]

Hannun YA, and Obeid LM (2008). Principles of bioactive lipid signalling: lessons from sphingolipids. Nature reviews. Molecular cell biology 9, 139–150. [PubMed: 18216770]

Heinz S, Benner C, Spann N, Bertolino E, Lin YC, Laslo P, Cheng JX, Murre C, Singh H, and Glass CK (2010). Simple combinations of lineage-determining transcription factors prime cis-regulatory elements required for macrophage and B cell identities. Molecular cell 38, 576–589. [PubMed: 20513432]

Herz J, Pardo J, Kashkar H, Schramm M, Kuzmenkina E, Bos E, Wiegmann K, Wallich R, Peters PJ, Herzig S, et al. (2009). Acid sphingomyelinase is a key regulator of cytotoxic granule secretion by primary T lymphocytes. Nature immunology 10, 761–768. [PubMed: 19525969]

Jin Y, Knudsen E, Wang L, Bryceson Y, Damaj B, Gessani S, and Maghazachi AA (2003). Sphingosine 1-phosphate is a novel inhibitor of T-cell proliferation. Blood 101, 4909–4915. [PubMed: 12586615]

Joshi NS, Cui W, Chandele A, Lee HK, Urso DR, Hagman J, Gapin L, and Kaech SM (2007). Inflammation directs memory precursor and short-lived effector CD8(+) T cell fates via the graded expression of T-bet transcription factor. Immunity 27, 281–295. [PubMed: 17723218]

Kappos L, Radue EW, O'Connor P, Polman C, Hohlfeld R, Calabresi P, Selmaj K, Agoropoulou C, Leyk M, Zhang-Auberson L, et al. (2010). A placebo-controlled trial of oral fingolimod in relapsing multiple sclerosis. The New England journal of medicine 362, 387–401. [PubMed: 20089952]

Kitatani K, Idkowiak-Baldys J, and Hannun YA (2008). The sphingolipid salvage pathway in ceramide metabolism and signaling. Cellular Signalling 20, 1010–1018. [PubMed: 18191382]

Kluk MJ, and Hla T (2001). Role of the Sphingosine 1-Phosphate Receptor EDG-1 in Vascular Smooth Muscle Cell Proliferation and Migration. Circulation Research 89, 496–502. [PubMed: 11557736]

Kovanen PE, and Leonard WJ (2004). Cytokines and immunodeficiency diseases: critical roles of the gamma(c)-dependent cytokines interleukins 2, 4, 7, 9, 15, and 21, and their signaling pathways. Immunological reviews 202, 67–83. [PubMed: 15546386]

Laplante M, and Sabatini DM (2012). mTOR signaling in growth control and disease. Cell 149, 274–293. [PubMed: 22500797]

Lee PP, Fitzpatrick DR, Beard C, Jessup HK, Lehar S, Makar KW, Pérez-Melgosa M, Sweetser MT, Schlissel MS, Nguyen S, et al. (2001). A Critical Role for Dnmt1 and DNA Methylation in T Cell Development, Function, and Survival. Immunity 15, 763–774. [PubMed: 11728338]

Lee SY, Kim JR, Hu Y, Khan R, Kim SJ, Bharadwaj KG, Davidson MM, Choi CS, Shin KO, Lee YM, et al. (2012). Cardiomyocyte specific deficiency of serine palmitoyltransferase subunit 2 reduces ceramide but leads to cardiac dysfunction. The Journal of biological chemistry 287, 18429–18439. [PubMed: 22493506]

Lee SY, Lee HY, Song JH, Kim GT, Jeon S, Song YJ, Lee JS, Hur JH, Oh HH, Park SY, et al. (2017). Adipocyte-Specific Deficiency of De Novo Sphingolipid Biosynthesis Leads to Lipodystrophy and Insulin Resistance. Diabetes 66, 2596–2609. [PubMed: 28698261]

Leonard WJ (1996). The molecular basis of X-linked severe combined immunodeficiency: defective cytokine receptor signaling. Annual review of medicine 47, 229–239.

Li M, Makkinje A, and Damuni Z (1996). The myeloid leukemia-associated protein SET is a potent inhibitor of protein phosphatase 2A. The Journal of biological chemistry 271, 11059–11062. [PubMed: 8626647]

Li Z, Kabir I, Tietelman G, Huan C, Fan J, Worgall T, and Jiang XC (2018). Sphingolipid de novo biosynthesis is essential for intestine cell survival and barrier function. Cell Death Dis 9, 173. [PubMed: 29415989]

Li Z, Li Y, Chakraborty M, Fan Y, Bui HH, Peake DA, Kuo MS, Xiao X, Cao G, and Jiang XC (2009). Liver-specific deficiency of serine palmitoyltransferase subunit 2 decreases plasma sphingomyelin and increases apolipoprotein E levels. The Journal of biological chemistry 284, 27010–27019. [PubMed: 19648608]

Liao Y, Smyth GK, and Shi W (2014). featureCounts: an efficient general purpose program for assigning sequence reads to genomic features. Bioinformatics 30, 923–930. [PubMed: 24227677]

Liu G, Burns S, Huang G, Boyd K, Proia RL, Flavell RA, and Chi H (2009). The receptor S1P1 overrides regulatory T cell-mediated immune suppression through Akt-mTOR. Nature immunology 10, 769–777. [PubMed: 19483717]

Liu G, Yang K, Burns S, Shrestha S, and Chi H (2010). The S1P1-mTOR axis directs the reciprocal differentiation of TH1 and Treg cells. Nature immunology 11, 1047–1056. [PubMed: 20852647]

Love MI, Huber W, and Anders S (2014). Moderated estimation of fold change and dispersion for RNA-seq data with DESeq2. Genome Biol 15, 550. [PubMed: 25516281]

Matloubian M, Lo CG, Cinamon G, Lesneski MJ, Xu Y, Brinkmann V, Allende ML, Proia RL, and Cyster JG (2004). Lymphocyte egress from thymus and peripheral lymphoid organs is dependent on S1P receptor 1. Nature 427, 355–360. [PubMed: 14737169]

Mendoza A, Fang V, Chen C, Serasinghe M, Verma A, Muller J, Chaluvadi VS, Dustin ML, Hla T, Elemento O, et al. (2017). Lymphatic endothelial S1P promotes mitochondrial function and survival in naive T cells. Nature 546, 158. [PubMed: 28538737]

Mukhopadhyay A, Saddoughi SA, Song P, Sultan I, Ponnusamy S, Senkal CE, Snook CF, Arnold HK, Sears RC, Hannun YA, and Ogretmen B (2009). Direct interaction between the inhibitor 2 and ceramide via sphingolipid-protein binding is involved in the regulation of protein phosphatase 2A

activity and signaling. FASEB journal: official publication of the Federation of American Societies for Experimental Biology 23, 751–763. [PubMed: 19028839]

Murphy SM, Ernst D, Wei Y, Laurà M, Liu Y-T, Polke J, Blake J, Winer J, Houlden H, Hornemann T, and Reilly MM (2013). Hereditary sensory and autonomic neuropathy type 1 (HSANI) caused by a novel mutation in SPTLC2. Neurology 80, 2106–2111. [PubMed: 23658386]

Nickels JT, and Broach JR (1996). A ceramide-activated protein phosphatase mediates ceramide-induced G1 arrest of Saccharomyces cerevisiae. Genes & development 10, 382–394. [PubMed: 8600023]

Novgorodov SA, Gudz TI, and Obeid LM (2008). Long-chain Ceramide Is a Potent Inhibitor of the Mitochondrial Permeability Transition Pore. Journal of Biological Chemistry 283, 24707–24717. [PubMed: 18596045]

Oh S, Perera LP, Terabe M, Ni L, Waldmann TA, and Berzofsky JA (2008). IL-15 as a mediator of CD4+ help for CD8+ T cell longevity and avoidance of TRAIL-mediated apoptosis. Proceedings of the National Academy of Sciences of the United States of America 105, 5201–5206. [PubMed: 18362335]

Ozcan U, Ozcan L, Yilmaz E, Duvel K, Sahin M, Manning BD, and Hotamisligil GS (2008). Loss of the tuberous sclerosis complex tumor suppressors triggers the unfolded protein response to regulate insulin signaling and apoptosis. Molecular cell 29, 541–551. [PubMed: 18342602]

Penno A, Reilly MM, Houlden H, Laura M, Rentsch K, Niederkofler V, Stoeckli ET, Nicholson G, Eichler F, Brown RH Jr., et al. (2010). Hereditary sensory neuropathy type 1 is caused by the accumulation of two neurotoxic sphingolipids. The Journal of biological chemistry 285, 11178–11187. [PubMed: 20097765]

Pircher H, Bürki K, Lang R, Hengartner H, and Zinkernagel RM (1989). Tolerance induction in double specific T-cell receptor transgenic mice varies with antigen. Nature 342, 559. [PubMed: 2573841]

Ridge JP, Di Rosa F, and Matzinger P (1998). A conditioned dendritic cell can be a temporal bridge between a CD4+ T-helper and a T-killer cell. Nature 393, 474–478. [PubMed: 9624003]

Rivera J, Proia RL, and Olivera A (2008). The alliance of sphingosine-1-phosphate and its receptors in immunity. Nature reviews. Immunology 8, 753–763.

Romero P, Zippelius A, Kurth I, Pittet MJ, Touvrey C, Iancu EM, Corthesy P, Devevre E, Speiser DE, and Rufer N (2007). Four Functionally Distinct Populations of Human Effector-Memory CD8+ T Lymphocytes. The Journal of Immunology 178, 4112–4119. [PubMed: 17371966]

Rotthier A, Auer-Grumbach M, Janssens K, Baets J, Penno A, Almeida-Souza L, Van Hoof K, Jacobs A, De Vriendt E, Schlotter-Weigel B, et al. (2010). Mutations in the SPTLC2 subunit of serine palmitoyltransferase cause hereditary sensory and autonomic neuropathy type I. American journal of human genetics 87, 513–522. [PubMed: 20920666]

Sallusto F, Nicolo C, De Maria R, Corinti S, and Testi R (1996). Ceramide inhibits antigen uptake and presentation by dendritic cells. The Journal of experimental medicine 184, 2411–2416. [PubMed: 8976196]

Sandhoff K (1993). Bioactive glycosphingolipids with differentiation-inducing activity toward leukemia cells. Jpn J Cancer Res 84, inside front cover.

Sawada S, Scarborough JD, Killeen N, and Littman DR (1994). A lineage-specific transcriptional silencer regulates CD4 gene expression during T lymphocyte development. Cell 77, 917–929. [PubMed: 8004678]

Scheffel MJ, Helke K, Lu P, Bowers JS, Ogretmen B, Garrett-Mayer E, Paulos CM, and Voelkel-Johnson C (2017). Adoptive Transfer of Ceramide Synthase 6 Deficient Splenocytes Reduces the Development of Colitis. Scientific reports 7, 15552. [PubMed: 29138469]

Schoenberger SP, Toes REM, van der Voort EIH, Offringa R, and Melief CJM (1998). T-cell help for cytotoxic T lymphocytes is mediated by CD40-CD40L interactions. Nature 393, 480–483. [PubMed: 9624005]

Seki A, and Rutz S (2018). Optimized RNP transfection for highly efficient CRISPR/Cas9-mediated gene knockout in primary T cells. The Journal of experimental medicine.

Siskind LJ, Kolesnick RN, and Colombini M (2002). Ceramide Channels Increase the Permeability of the Mitochondrial Outer Membrane to Small Proteins. Journal of Biological Chemistry 277, 26796–26803. [PubMed: 12006562]

Siskind LJ, Kolesnick RN, and Colombini M (2006). Ceramide forms channels in mitochondrial outer membranes at physiologically relevant concentrations. Mitochondrion 6, 118–125. [PubMed: 16713754]

Sofi MH, Heinrichs J, Dany M, Nguyen H, Dai M, Bastian D, Schutt S, Wu Y, Daenthanasanmak A, Gencer S, et al. (2017). Ceramide synthesis regulates T cell activity and GVHD development. JCI Insight 2.

Sokke Umeshappa C, Hebbandi Nanjundappa R, Xie Y, Freywald A, Deng Y, Ma H, and Xiang J (2012). CD154 and IL-2 signaling of CD4+ T cells play a critical role in multiple phases of CD8+ CTL responses following adenovirus vaccination. PloS one 7, e47004. [PubMed: 23071696]

Tettamanti G, Bassi R, Viani P, and Riboni L (2003). Salvage pathways in glycosphingolipid metabolism. Biochimie 85, 423–437. [PubMed: 12770781]

Wang R, Dillon CP, Shi LZ, Milasta S, Carter R, Finkelstein D, McCormick LL, Fitzgerald P, Chi H, Munger J, and Green DR (2011). The transcription factor Myc controls metabolic reprogramming upon T lymphocyte activation. Immunity 35, 871–882. [PubMed: 22195744]

Wilson EB, and Livingstone AM (2008). Cutting edge: CD4+ T cell-derived IL-2 is essential for help-dependent primary CD8+ T cell responses. J Immunol 181, 7445–7448. [PubMed: 19017930]

Zamzami N, Marchetti P, Castedo M, Decaudin D, Macho A, Hirsch T, Susin SA, Petit PX, Mignotte B, and Kroemer G (1995). Sequential reduction of mitochondrial transmembrane potential and generation of reactive oxygen species in early programmed cell death. The Journal of experimental medicine 182, 367–377. [PubMed: 7629499]

Zeng H, Yang K, Cloer C, Neale G, Vogel P, and Chi H (2013). mTORC1 couples immune signals and metabolic programming to establish T(reg)-cell function. Nature 499, 485–490. [PubMed: 23812589]

HIGHLIGHTS

- $CD8^+$ T cell function and survival is impaired in HSAN-I patients with *SPTLC2* mutation
- Mouse $CD8^+$ T cells require SPTLC2 to protect against viral infections
- SPTLC2-mediated sphingolipid synthesis prevents mTORC1 hyperactivation and cell death
- Sphingolipid supplementation restores SPTLC2-deficient $CD8^+$ T cell effector function

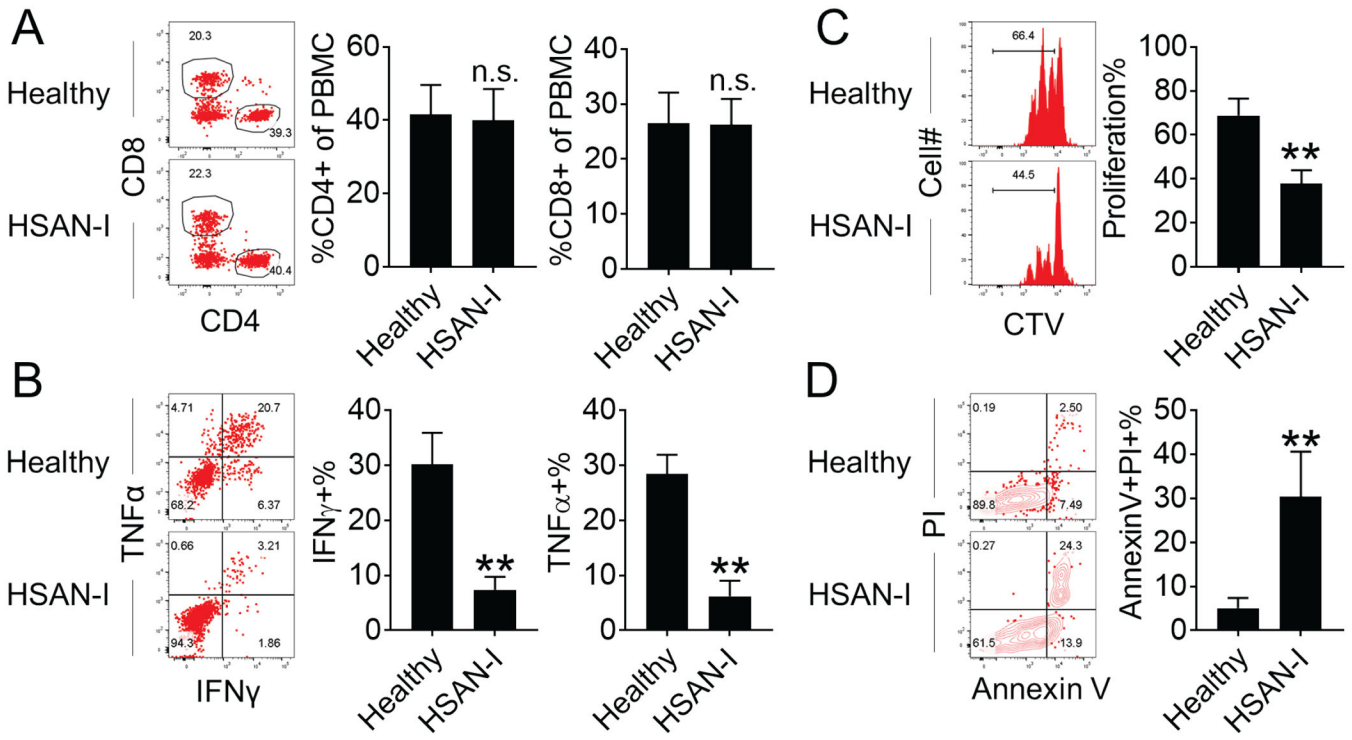

Figure 1. The *SPTLC2* mutations affect HSAN-I patient CD8$^+$ T cell effector cytokine production, proliferation, and survival.

(A) FACS dot plots and bar graphs show the percentages of CD4$^+$ and CD8$^+$ T cells in PBMCs from HSAN-I patients and healthy subjects.

(B) PBMCs from HSAN-I patients and healthy subjects were stimulated with PMA and ionomycin for 6 hours in the presence of brefeldin A before FACS analysis of IFNγ- and TNFα-producing CD8$^+$ T cells.

(C-D) PBMCs from HSAN-I patients and healthy subjects were labeled with Celltrace Violet (CTV) and stimulated with anti-CD2, anti-CD3 and anti-CD28 for 3 days before FACS analysis. FACS plots and bar graphs show the percentages of proliferating (C) and apoptotic (D) CD8$^+$ T cells.

Data are expressed as mean ± SD and cumulative of three independent experiments (ten pairs of samples for each experiment described in A-D). **p<0.01; n.s., not significant. See also Figure S1.

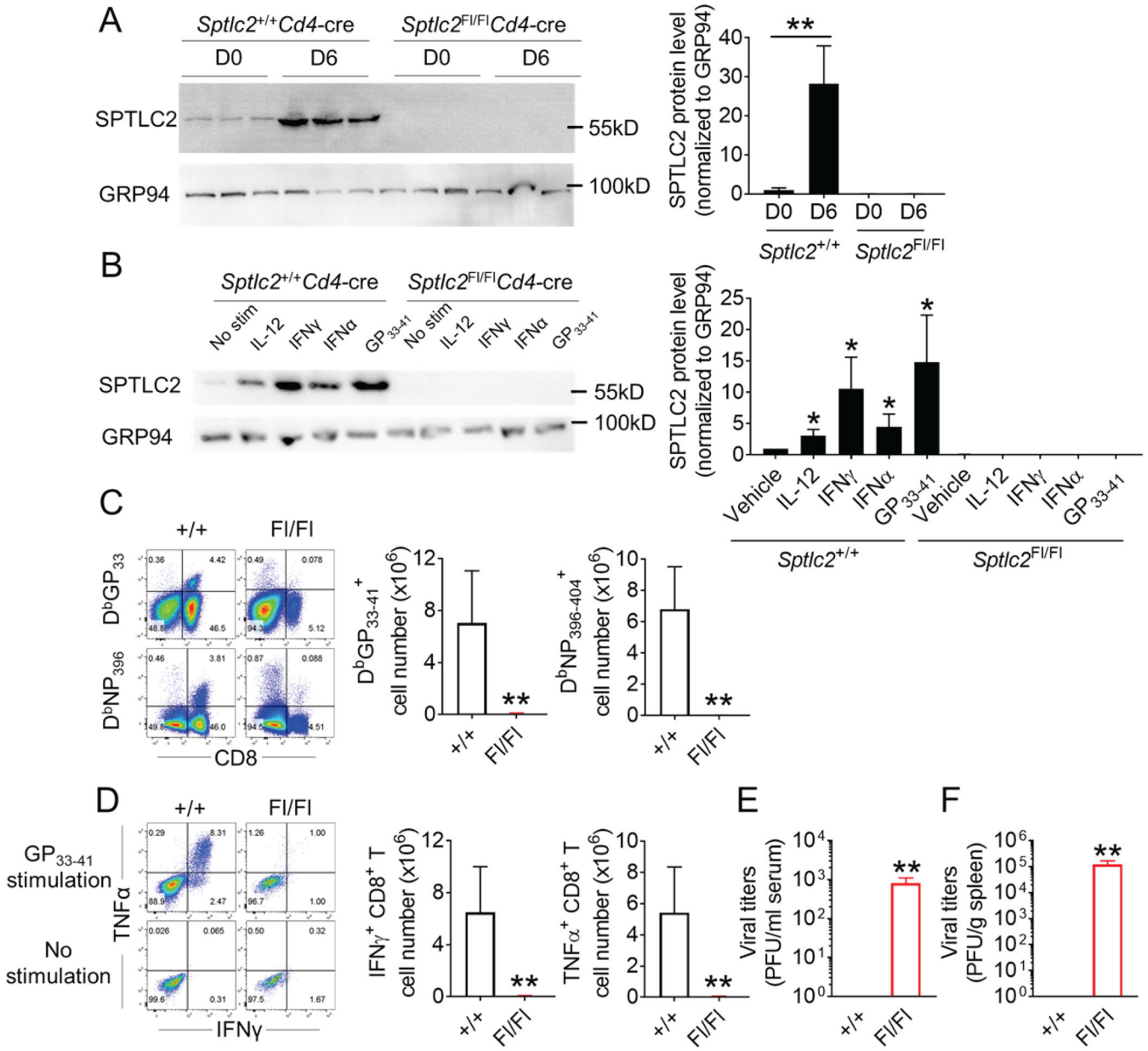

Figure 2. *Sptlc2*-deficiency impairs antiviral effector CD8$^+$ T cell formation.

(A) Antigen-specific P14 CD8$^+$ T cells were purified on day 6 (D6) after LCMV-Armstrong infection from the “P14 chimeric mice”. Naïve P14 T cells were also purified before LCMV infection (D0) to analyze the basal level of SPTLC2 protein by western blot. *Sptlc2*-deficient P14 CD8$^+$ T cells were included as negative controls. Bar graphs show the densitometry quantification of the SPTLC2 immunoblot bands. GRP94 was used as a loading control.

(B) P14 TCR transgenic mouse splenocytes were stimulated with $GP_{33–41}$ peptide or various cytokines as indicated for 3 days for immunoblot. Each lane represents an individual mouse sample (A-B).

(C-F) *Sptlc2*$^{Flox/Flox}$*Cd4*-cre (Fl/Fl) mice and wildtype littermates (+/+) were infected with LCMV-Armstrong and sacrificed 8 days later. Representative FACS plots and bar graphs (C-

D) show the percentages and numbers of $D^bGP_{33–41}$ and $D^bNP_{396–404}$ tetramer-positive splenic *Sptlc2*-deficient or wildtype $CD8^+$ T cells (C), the effector cytokine-producing $CD8^+$ T cells after restimulation with or without the LCMV peptide $_{GP33–41}$ for 6 hours (D) and viral titers in mouse serum (E) and spleens (F).

Data are expressed as mean ± SD (error bars) and are representative of two (six (A) or three (B) pairs of mice in total) or three (C-F, eight pairs of mice in total) independent experiments (three in each experiment). *p<0.05; **p<0.01. See also Figure S2.

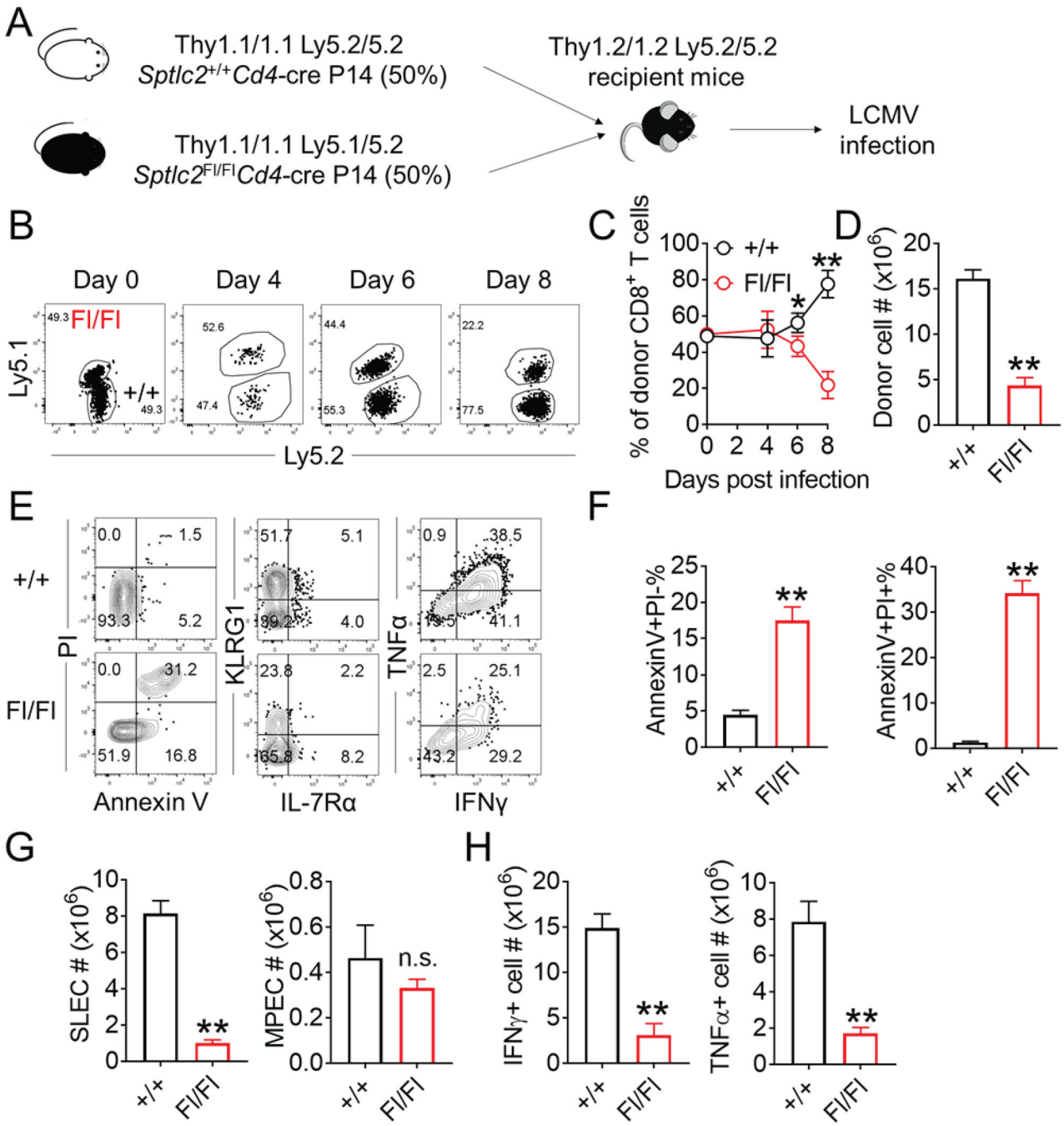

Figure 3. CD8$^+$ T cells require cell-intrinsic SPTLC2 expression for robust effector T cell responses.

(A-D) Congenically mismatched *Sptlc2*$^{Flox/Flox}$*Cd4*-cre and *Sptlc2*$^{+/+}$*Cd4*-cre P14 CD8$^+$ T cells (10^4 cells each) were mixed and adoptively transferred into B6 recipient mice, which were subsequently infected with LCMV-Armstrong (A). The percentages (B-C) and numbers (D, day 8) of *Sptlc2*-sufficient (WT) and -deficient donor CD8$^+$ T cells are shown. (E-H) FACS plots and bar graphs show the percentages or numbers of apoptotic CD8$^+$ T cells (E and F), SLECs and MPECs (E and G), and cytokine-producing CD8$^+$ T cells (E and

H). Data (C, D, F-H) are expressed as mean ± SD (error bars) and cumulative of three independent experiments (six to eight mice in total). *p<0.05; **p<0.01; n.s., not significant.

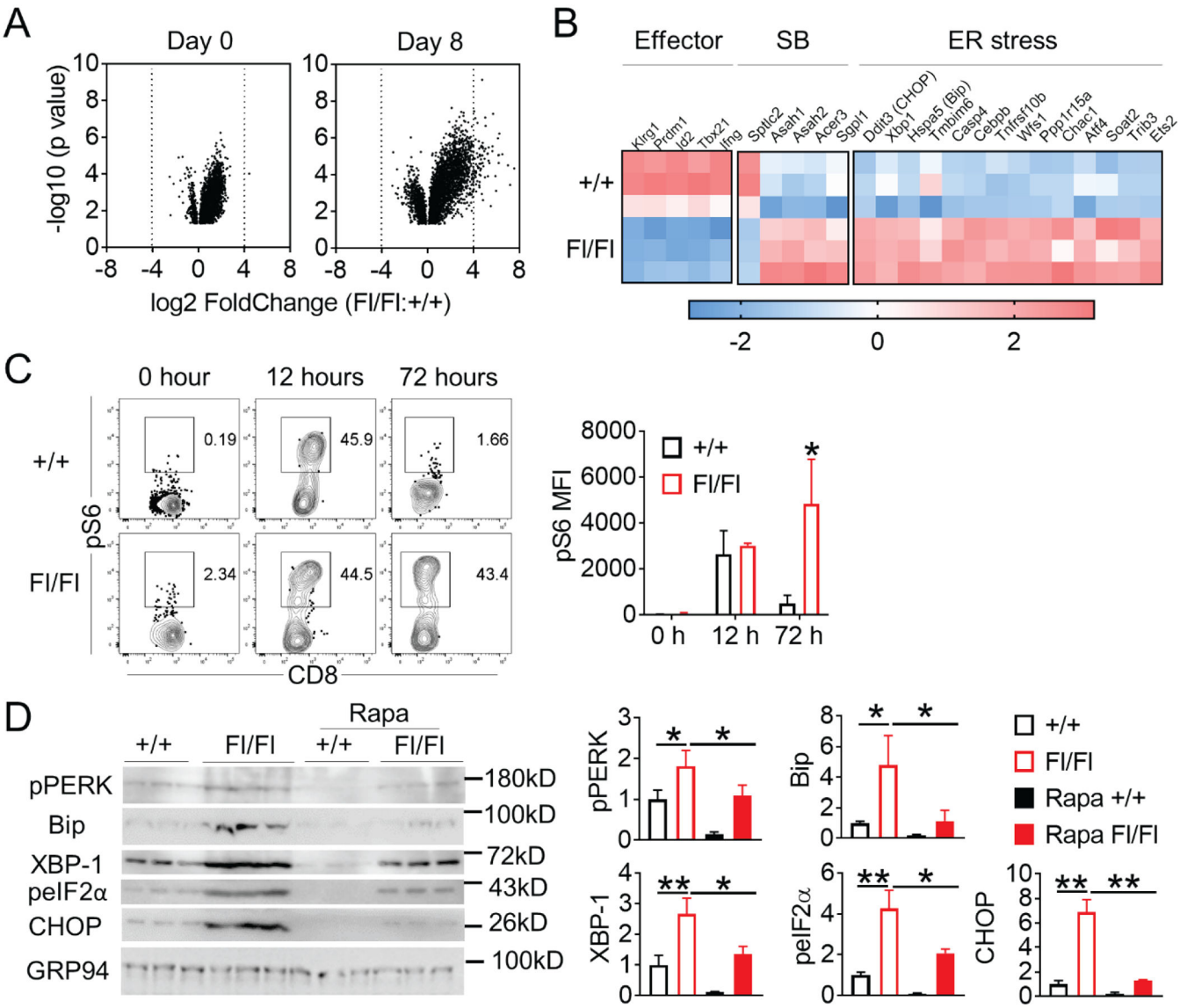

Figure 4. *Sptlc2*-deficiency causes aberrant mTORC1 activation and ER stress in antiviral CD8$^+$ T cells.

(A) Volcano plots show the distribution of significantly up- and down-regulated genes in the *Sptlc2*-deficient CD8$^+$ T cells before and 8 days after LCMV-Armstrong infection.

(B) A heat map shows the z-score of the mRNA levels of the indicated genes in CD8$^+$ T cells purified from three pairs of *Sptlc2*$^{Flox/Flox}$*Cd4*-cre (Fl/Fl) mice and wildtype littermates (+/+) at day 8 after LCMV-Armstrong infection. “Effector” block contains hallmark genes of effector CD8$^+$ T cells. Genes regulating the sphingoid base salvage pathways and ER-stress are shown in the “SB” and “ER stress” blocks. *Sptlc2* is included as a control.

(C) FACS plots show the percentages of phosphorylated S6 (pS6) in *Sptlc2*-sufficient (+/+) and -deficient (Fl/Fl) CD8$^+$ T cells after *in vitro* stimulation with anti-CD3 and anti-CD28. pS6 MFI is expressed as mean ± SD (error bars) and cumulative of three independent experiments (one pair of mice in each experiment).

(D) The ER stress marker expression in $CD8^+$ T cells of *Sptlc2*$^{Flox/Flox}$*Cd4*-cre (Fl/Fl) and *Sptlc2*$^{+/+}$*Cd4*-cre (+/+) littermate mice infected with LCMV-Armstrong 8 days earlier was analyzed by western blot. Rapamycin was administered every other day (100 μg/kg body weight) as indicated. T cells of three mice in each group were collected separately from two independent infection experiments and analyzed together. Each lane represents an individual sample. Bar graphs show the densitometry quantification of the immunoblot bands. Data are expressed as mean ± SD (error bars). *$p<0.05$; **$p<0.01$. See also Figure S3.

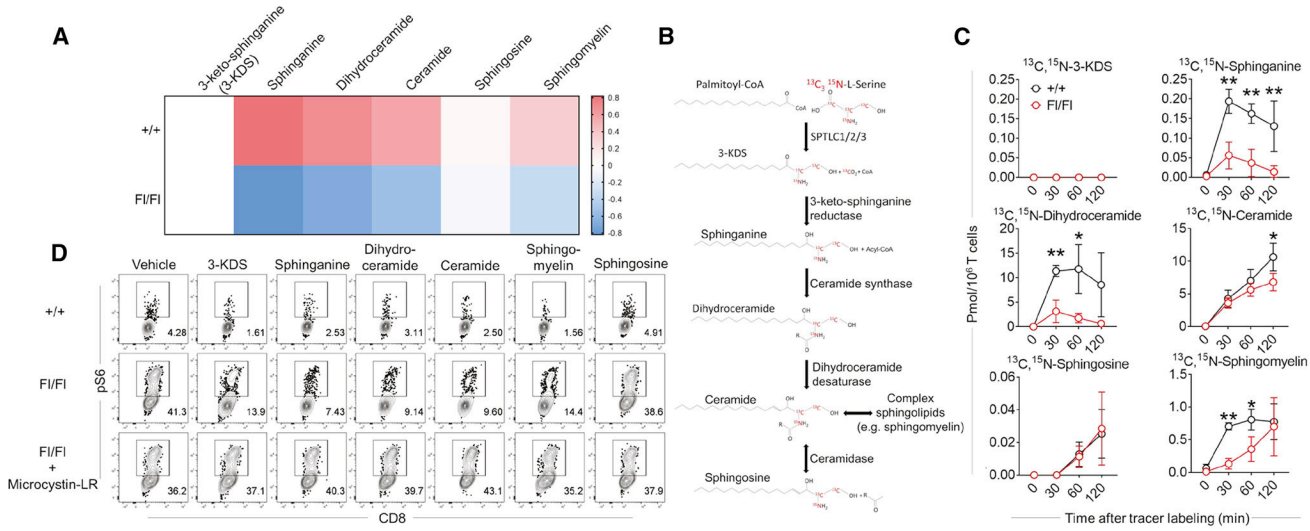

Figure 5. *Sptlc2*-deficiency reduces sphingolipid biosynthetic flux and prolongs mTORC1 activation through protein phosphatases in CD8$^+$ T cells.

(A) *Sptlc2*$^{Flox/Flox}$*Cd4*-cre (Fl/Fl) or *Sptlc2*$^{+/+}$*Cd4*-cre (+/+) P14 CD8$^+$ T cells were cultured with the cognate peptide $GP_{33–41}$ for 3 days. The primed CD8$^+$ T cells were then expanded using IL-2 for another 2 days before lipid extraction and mass spectrometry analysis of sphingolipids. The heat map shows the z-score of the indicated metabolites.

(B) The sphingolipid *de novo* synthetic pathway is depicted with tracers highlighted in red.

(C) P14 CD8$^+$ T cells as described in (A) were expanded using IL-2. Then T cells were washed and cultured in HBSS plus 1% FBS in the presence of isotope-labeled L-serine for 0~120 minutes for mass spectrometry analysis of the tracer incorporation into various sphingolipids.

(D) *Sptlc2*$^{Flox/Flox}$*Cd4*-cre (Fl/Fl) or *Sptlc2*$^{+/+}$*Cd4*-cre (+/+) CD8$^+$ T cells were stimulated with anti-CD3 and anti-CD28 for 3 days in the presence or absence of sphingolipids (5 μM 3-KDS, 5 μM sphinganine, 50 nM C16 ceramide, 50 nM C18 dihydroceramide, 4 μg/ml palmitoyl sphingomyelin, and 1 μM sphingosine) or microcystin-LR (it inhibits both PP1 and PP2A at 25 nM) as indicated before FACS analysis of pS6.

Data (A and C, two pairs of mice in each experiment) are cumulative of two independent experiments or representative (D, one pair of mice in each experiment) of three experiments. Data are expressed as mean ± SD (error bars) (C). *p<0.05; **p<0.01. See also Figure S4, S5 and S6.

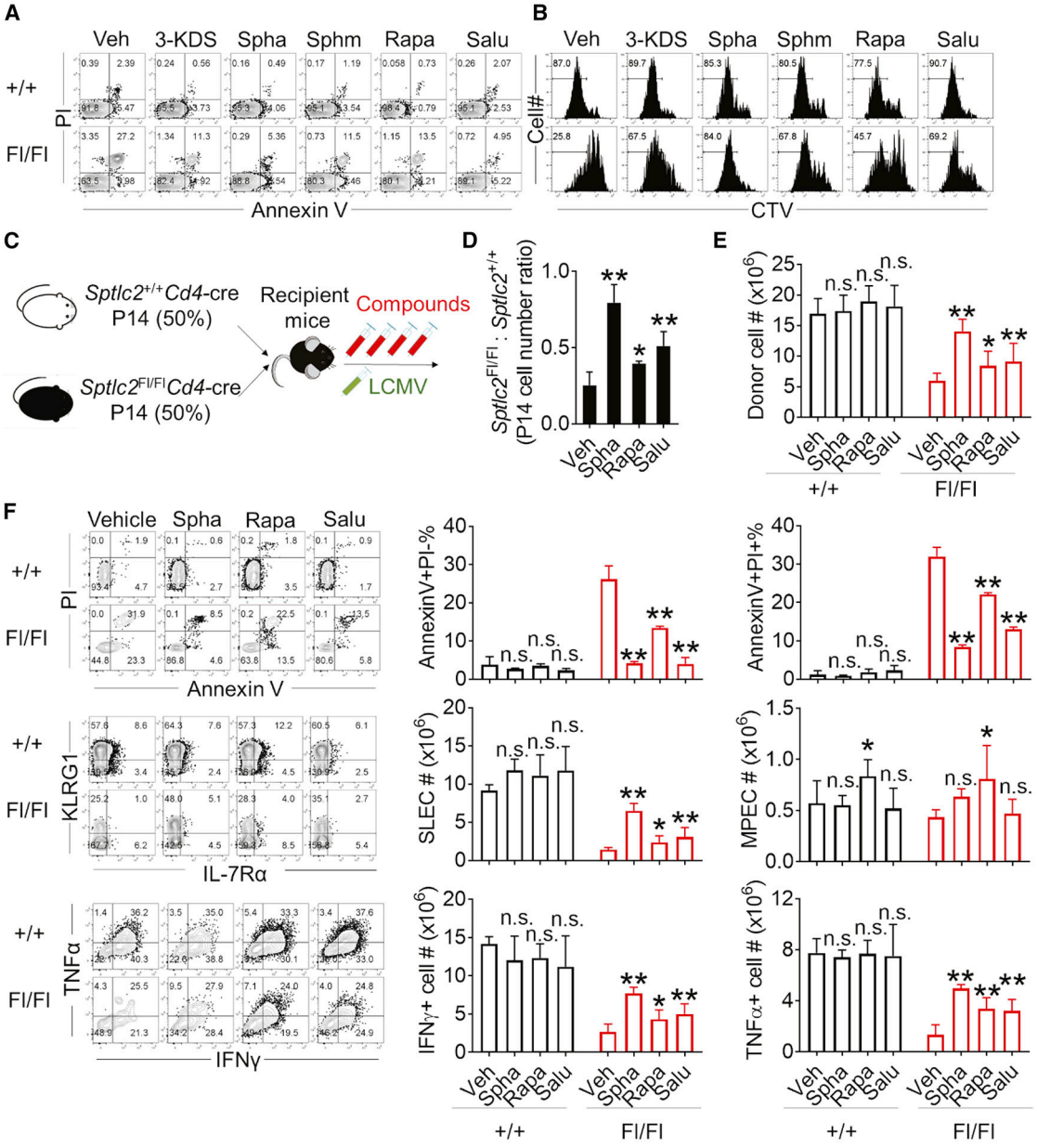

Figure 6. Sphingolipid supplementation and inhibition of ER stress-induced cell death partially restore *Sptlc2*-deficient antiviral T cell survival and expansion.

(A-B) *Sptlc2*$^{Flox/Flox}$*Cd4*-cre (Fl/Fl) or *Sptlc2*$^{+/+}$*Cd4*-cre (+/+) CD8^{+} T cells were labeled with (B) or without (A) CTV and stimulated with anti-CD3 and anti-CD28 for 3 days in the presence or absence of 3-keto-sphinganine (3-KDS, 5 μM), sphinganine (Spha, 5 μM), sphingomyelin (Sphm, 4 μg/ml), rapamycin (Rapa, 10 nM), and salubrinal (Salu, 5 μM) before FACS analysis of apoptosis (A) and proliferation (B).

(C-E) *Sptlc2*$^{Flox/Flox}$*Cd4*-cre (Fl/Fl) and wildtype P14 CD8^{+} T cells from littermates were mixed (1×10^{4} cells from either group) and adoptively transferred into C57BL/6 mice, which were infected with LCMV and sacrificed 8 days later. Sphinganine (100 μg/kg), rapamycin (100 μg/kg), and salubrinal (1 mg/kg) were peritoneally injected every other day (day 0~8

after LCMV infection). Bar graphs show the ratio (D) and total numbers (E) of *Sptlc2*-deficient and -sufficient donor $CD8^+$ splenic T cells at day 8 after LCMV infection. (F) FACS plots and bar graphs show the percentages or numbers of apoptotic $CD8^+$ T cells, SLECs and MPECs, and cytokine-producing $CD8^+$ T cells. Data are representative (A-B, three pairs of mice in total) and cumulative (D-F, six pairs of mice in total) of three independent experiments. Data are expressed as mean ± SD (error bars) (D-F). *$p<0.05$; **$p<0.01$; n.s., not significant. See also Figure S4 and S5.

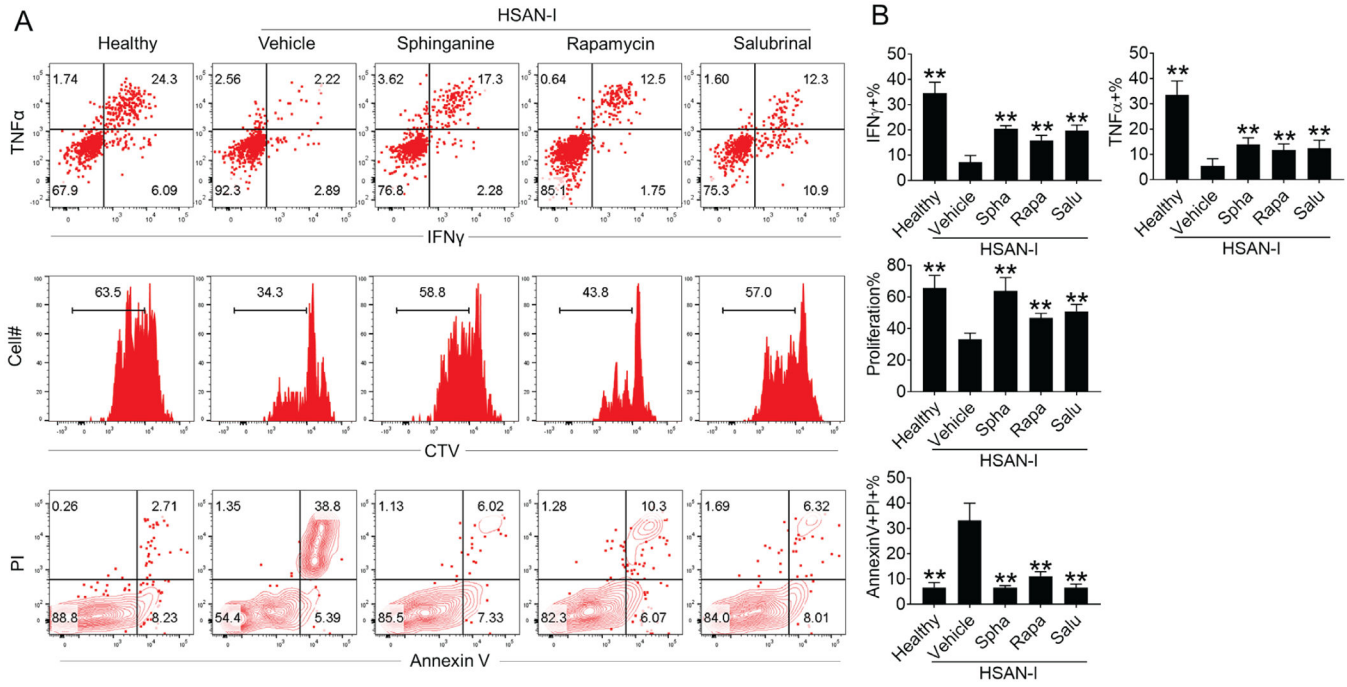

Figure 7. Supplementing with sphinganine and inhibiting ER stress-induced cell death corrects the immunodeficiency in *SPTLC2*-mutated HSAN-I patient PBMCs.

(A) PBMCs from HSAN-I patients and healthy subjects were stimulated with PMA and ionomycin for 6 hours in the presence or absence of the indicated compounds (upper panel). FACS plots show the production of IFNγ and TNFα by $CD8^+$ T cells. Alternatively, PBMCs were labeled with CTV (middle panel only) and stimulated with anti-CD2, anti-CD3 and anti-CD28 for 3 days (both middle and lower panels). FACS plots show the percentages of proliferating (middle panel) and apoptotic (lower panel) $CD8^+$ T cells.

(B) Bar graphs show the cumulative results obtained from ten pairs of samples. Data are expressed as mean ± SD. **p<0.01. See also Figure S7.

KEY RESOURCES TABLE

REAGENT RESOURCE	SOURCE	IDENTIFIER
Antibodies		
PerCP anti-human CD8a	BioLegend	BioLegend Cat# 300922, RRID:AB_1575072
APC/Cy7 anti-human CD4	BioLegend	BioLegend Cat# 357416, RRID:AB_2616810
PE anti-human CD197 (CCR7)	BioLegend	BioLegend Cat# 353204, RRID:AB_10913813
APC anti-human CD45RA	BioLegend	BioLegend Cat# 304112, RRID:AB_314416
PE/Cy7 anti-human IFN-γ	BioLegend	BioLegend Cat# 502528, RRID:AB_2123323
PE anti-human TNF-α	BioLegend	BioLegend Cat# 502909, RRID:AB_315261
PerCP/Cy5.5 anti-mouse CD8a	BioLegend	BioLegend Cat# 100734, RRID:AB_2075238
APC/Cy7 anti-mouse/human CD44	BioLegend	BioLegend Cat# 103028, RRID:AB_830785
Brilliant Violet 421™ anti -rat CD90/mouse CD90.1	BioLegend	BioLegend Cat# 202529, RRID:AB_10899572
APC/Cy7 anti-rat CD90/mouse CD90.1 (Thy-1.1)	BioLegend	BioLegend Cat# 202520, RRID:AB_2303153
FITC anti-mouse CD8a	BioLegend	BioLegend Cat# 100804
PE anti-mouse CD8b	BioLegend	BioLegend Cat# 126608, RRID:AB_961298
Rat Anti-Mouse CD90.2 Monoclonal, FITC	Miltenyi Biotec	Miltenyi Biotec Cat# 130-091-602, RRID:AB_244295
APC anti-mouse CD45.1	BioLegend	BioLegend Cat# 110714, RRID:AB_313503
PE anti-mouse CD45.2	BioLegend	BioLegend Cat# 109808, RRID:AB_313445
PE/Cy7 anti-mouse KLRG1	BioLegend	BioLegend Cat# 138416
APC anti-mouse CD127 (IL-7Rα)	BioLegend	BioLegend Cat# 121122
Annexin V-FITC Kit	BioLegend	Miltenyi Biotec Cat# 130-092-052
PE/Cy7 anti-mouse IFN-γ	BioLegend	BioLegend Cat# 505826, RRID:AB_2295770
PE anti-mouse TNF-α	BioLegend	BioLegend Cat# 506306, RRID:AB_315427
Rabbit Anti-eIF2alpha, phosphor (Ser51) mAb	Cell Signaling Technology	Cell Signaling Technology Cat# 3597, RRID:AB_390740
Phospho-S6 Ribosomal Protein (Ser235/236) (D57.2.2E) mAb	Cell Signaling Technology	Cell Signaling Technology Cat# 4858, RRID:AB_916156
BiP (C50B12) Rabbit mAb	Cell Signaling Technology	Cell Signaling Technology Cat# 3177P, RRID:AB_10828008
CHOP (D46F1) Rabbit mAb	Cell Signaling Technology	Cell Signaling Technology Cat# 5554S, RRID:AB_10694399
XBP-1s (D2C1F) Rabbit mAb	Cell Signaling Technology	Cell Signaling Technology Cat# 12782, RRID:AB_2687943

REAGENT RESOURCE	SOURCE	IDENTIFIER
Phospho-PERK (Thr980) (16F8) Rabbit mAb	Cell Signaling Technology	Cell Signaling Technology Cat# 3179S, RRID:AB_2095853
SPTLC2 (C-term) antibody	OriGene	Cat# TA319780
Phosphor-NF-kB p65 Ser536 (93H1) Rabbit mAb antibody	Cell Signaling Technology	Cell Signaling Technology Cat# 3033
Phospho-p38 MAPK (Thr180/Tyr182) (D3F9) XP® Rabbit mAb	Cell Signaling Technology	Cell Signaling Technology Cat# 4511
Phospho-SAPK/JNK (Thr183/Tyr185) (81E11) Rabbit mAb	Cell Signaling Technology	Cell Signaling Technology Cat# 4668
Phospho-p44/42 MAPK (Erk1/2) (Thr202/Tyr204) (D13.14.4E) XP® Rabbit mAb	Cell Signaling Technology	Cell Signaling Technology Cat# 4370,
Phospho-Akt (Ser473) (D9E) XP® Rabbit mAb	Cell Signaling Technology	Cell Signaling Technology Cat# 4060,
Phospho-Akt (Thr308) Antibody	Cell Signaling Technology	Cell Signaling Technology Cat# 9275
Phospho-4E-BP1 (Ser65) Antibody	Cell Signaling Technology	Cell Signaling Technology Cat# 9451
GRP94 antibody	Cell Signaling Technology	Cell Signaling Technology Cat# 20292,
HRP Donkey anti-rabbit IgG	BioLegend	Cat# 406401
LEAF™ Purified anti -mouse CD3	BioLegend	Cat# 100223
Ultra-LEAF™ Purified anti -mouse CD28	BioLegend	Cat# 102116
LEAF™ Purified anti -human CD2	BioLegend	Cat# 309212
LEAF™ Purified anti-human CD28	BioLegend	Cat# 302923
LEAF™ Purified anti -human CD3	BioLegend	Cat# 317315
Chemicals, Peptides, and Recombinant Proteins		
Agarose, low melting	Thermo Fischer	Cat# 10377033
Rapamycin	Enzo Life Sciences	Cat# BML-A275–0005
Salubrinal	Santa Cruz	Cat# sc-202332
Microcystin LR	Focus Biomolecules	Cat# 10–2719
3-keto-sphinganine	Abcam	Cat# ab144107
D-erythro Sphinganine	Cayman Chemical	Cat# 10007945–50
C18-dihydro-ceramide (n-stearoyl-)	Promochem	Cat# LA 56-1077-4
C16 Ceramide (N-Palmitoylsphingosine, D-erythro)	Santa Cruz	Cat# sc-201379
Sphingosine	Echelon Biosciences	Cat# S-1000
Sphingosine-1-phosphate	Echelon Biosciences	Cat# 10–4526
Palmitoyl Sphingomyelin	Cayman Chemical	Cat# 10007946–1
Ficoll	Sigma-Aldrich	Cat# F2637
1-deoxysphinganine	Avanti Polar Lipids	Cat# 860493
1-deoxymethylsphinganine	Avanti Polar Lipids	Cat# 860473
Percoll	Sigma-Aldrich	Cat# 17-0891-01
Clarity Western ECL Substrate	Bio-Rad Laboratories	Cat# 1705061
Fixation Buffer	BioLegend	Cat# 420801
HBSS	GIBCO	Cat# 14175129
PBS	GIBCO	Cat# 20012–068
L-Glutamine	GIBCO	Cat# 25030–024

REAGENT RESOURCE	SOURCE	IDENTIFIER
RPMI 1640 Medium	GIBCO	Cat# 21875034
Non-essential amino acids	GIBCO	Cat# 11140–035
Fetal bovine serum	Sigma-Aldrich	Cat# F0804
CellTrace ™ Violet	Thermo Fischer	Cat# C34557
$^{13}C_3$, ^{15}N-L-Serine	Sigma-Aldrich	Cat# 608130
GP (33–41) peptide	GenScript	Cat# RP20091
Recombinant Mouse IL-2	BioLegend	Cat# 575408
Recombinant Mouse IL-12 (p70)	BioLegend	Cat# 577004
IFN-gamma	PeproTech	Cat# 315-05-20
IFN-alpha	PeproTech	Cat# 300–02A
$D^bGP_{33–41}$ tetramer	NIH tetramer core facility	Task# 31755
$D^bNP_{396–404}$ tetramer	NIH tetramer core facility	Task# 31756
Other resources		
PVDF membrane	Santa Cruz	Cat# sc-358811
RNeasy Mini Kit	QIAGEN	Cat# 74106
RNase-Free DNase Set	QIAGEN	Cat# 79254
Experimental Models: Organisms/Strains		
LCMV-Armstrong	(Dutko and Oldstone, 1983)	Strain# CA1371
Mouse: C57BL/6N	Charles River	Strain# 027
Mouse: SPTLC2tm2.1Jia	(Li et al., 2009)	MGI:4414752
Mouse: Tg(TcrLCMV)327Sdz (P14)	(Pircher et al., 1989)	MGI:2665105
Mouse: Tg(Cd4-cre)1Cwi/BfluJ	(Lee et al., 2001; Sawada et al., 1994)	JAX Strain# 017336
Software and Algorithms		
Flowjo	FlowJo, LLC	https://www.flowjo.com/
ImageJ	NIH	https://imagej.nih.gov/ij/
Deposited data		
RNA-seq data		GEO: GSE112715